STATE OF POLAR CLIMATE

2025

CHINESE ACADEMY OF METEOROLOGICAL SCIENCES

STATE OF POLAR CLIMATE

(2025)

CHINESE ACADEMY OF METEOROLOGICAL SCIENCES

2026.03

Editorial Committee for State of Polar Climate 2025

Abstract

In 2025, the overall temperature of the Antarctic continent was relatively high, with obvious seasonal variations and concentrated regional warm anomalies. In 2025, the annual average temperature of the Antarctic continent was -31.29°C, 0.55°C higher than the climatological average. Spring, summer and autumn all exhibited warm anomalies, with the strongest warming in spring: temperatures were 2.14°C above normal, while winter showed a cold anomaly, 0.63°C below normal.Warmer regions were mainly concentrated in West Antarctica (including the Antarctic Peninsula), East Antarctic Dome, Queen Maud Land and coastal Victoria Land. Only local areas in Wilkes Land and the western Ross Sea were colder than normal.The strongest winter warming occurred over the Antarctic Peninsula and Victoria Land, while peak spring warming was observed in regions such as the East Antarctic Dome.The annual average temperatures at Rothera Station, San Martín Station and Novolazarevskaya Station set historical records, and another 8 stations ranked second or third highest in their historical records.

The Arctic region continued its accelerated warming trend, with the Barents Sea and its surrounding areas as the core region of the strongest warming. In 2025, the annual average temperature of the Arctic was -6.40°C, 1.14°C higher than the climatological average.The average temperatures in winter, spring, summer and autumn were -17.75°C, -9.37°C, 6.43°C and -4.60°C respectively, all showing warm anomalies.The warming magnitudes were strongest in winter and autumn, with anomalies of 2.13°C and 1.78°C respectively.The Barents Sea and adjacent areas became the core region of extreme warming.The annual average temperatures at Bodoe (Norway) and Teriberka (Russia) set historical records.Temperatures at Thule (Greenland) and NyÅlesund (Norway) were among the highest anomalies. Historical temperature records were broken in winter and summer at many locations.Sea surface temperature (SST) monitoring shows that in 2025, the Arctic Ocean SST was dominated by warm anomalies overall, accompanied by significant seasonal and regional differences.In August, the Arctic sea surface temperature reached the second highest level in history, and the Kara Sea set a record high for regional sea surface temperature.

In 2025, polar sea ice exhibited a persistent shrinking trend, with numerous indices of sea ice extent in both the Antarctic and Arctic reaching or approaching historical extremes. On 1 March 2025, Antarctic sea ice extent declined to its annual minimum of 1.96×10^6 km^2, while the annual maximum reached 17.85×10^6 km^2. The annual mean, annual minimum, and annual maximum sea ice extents all ranked as the third lowest since the initiation of satellite observations in 1979. Arctic sea ice shrinkage was even more substantial. In 2025, the annual maximum Arctic sea ice extent of 14.35×10^6 km^2 marked a 47-year record low, and the annual mean of 10.13×10^6 km^2

established a new historical minimum. The annual minimum sea ice extent ranked the tenth lowest in the observational record.Sea ice extent during multiple months of the winter half-year broke historical minima for the corresponding periods.

In 2025, the Antarctic ozone hole moderated relative to its previous strong depletion state, while the Arctic experienced a relatively severe ozone depletion event in recent decades. In 2025, the maximum daily area of the Antarctic ozone hole was approximately 22.86 million km², ranking the fifth smallest in the observational record.The average area during the peak period was smaller than the climatological mean, and the ozone hole closed completely by late November, about three weeks earlier than the average over the past decade.In the Arctic, an unusually strong and persistent polar vortex from winter 2024 to early spring 2025 led to significant ozone depletion. In March 2025, total column ozone over the Arctic was substantially lower than normal, with a pronounced ozone minimum over Scandinavia and northern Eurasia.2025 stands as one of the most severe years for Arctic ozone depletion in recent decades, in sharp contrast to the record-high ozone concentrations observed in the same period of 2024.

In the polar regions, the concentrations of major greenhouse gases in the atmosphere are consistent with the global trend, showing a steady and continuous rise. As of 2024, the annual average concentrations of carbon dioxide, methane, nitrous oxide, and sulfur hexafluoride in the Antarctic atmosphere were 419.99 ppm, 1876.50 ppb, 336.80 ppb, and 11.55 ppt, respectively;the corresponding annual average concentrations in the Arctic atmosphere were 426.13 ppm, 2024.33 ppb, 338.06 ppb, and 12.05 ppt, respectively.Compared with 2023, the average concentrations of the four major greenhouse gases in the polar regions all increased,among which the annual increments in sulfur hexafluoride concentrations at both the Antarctic and Arctic reached record highs.

Contents

Chapter 1 Air Temperature and Pressure

1.1 Air Temperature

1.1.1 Antarctic

The analysis in this subsection is based on surface air temperature (SAT) observations from multiple stations across Antarctica, along with the first-generation Global Atmospheric Reanalysis Dataset (CMA-RA) released by the National Meteorological Information Center of the China Meteorological Administration (CMA). The SAT observations from Great Wall Station and Zhongshan Station were provided by the Chinese Academy of Meteorological Sciences and National Arctic and Antarctic Data Center(NADC), while data from other stations were sourced from the Antarctic Reference Dataset for Environmental Research (Met-READER), compiled by the British Antarctic Survey. All datasets have undergone rigorous quality control to ensure the accuracy and reliability of the analysis.

The results indicate that the annual mean SAT over the Antarctic continent in 2025 was –31.29°C, which is 0.55°C above the climatological normal. Seasonally, the mean SAT values for austral summer (December–February), autumn (March–May), winter (June–August), and spring (September–November) were –20.87°C, –35.00°C, –38.88°C, and –30.25°C, respectively. Notably, the Antarctic continent experienced warmer-than-normal conditions in summer, autumn, and spring of 2025, with anomalies of 0.74°C, 0.10°C, and 2.14°C, respectively; winter, however, exhibited a cold anomaly of –0.63°C.

Spatially, most of Antarctica recorded SATs above the climatological normal in 2025. The primary warming hotspots included West Antarctica (including the Antarctic Peninsula), the Dome regions of East Antarctica, Dronning Maud Land, and coastal areas of Victoria Land (Figure 1.1). Only isolated areas—such as Wilkes Land and the western coast of the Ross Sea—showed below-normal SATs. Against this backdrop, three stations (Rothera, San Martin, and Novolazarevskaya) recorded their highest annual SAT on record; four stations (Great Wall, O'Higgins, Faraday, and Syowa) registered their second-highest; and another four (Bellingshausen, Palmer, Marble Point, and Manuela) marked their third-highest.

In 2025, the Antarctic Peninsula exhibited a warm SAT anomaly beginning in autumn. The autumn mean SAT at five stations in this region ranked among the top three highest on record, with O'Higgins Station reaching a record high (1.98°C above normal). The warm anomaly intensified in winter, during which all nine stations recorded winter mean SAT among the top three highest on record; Rothera and San Martin Stations set new records, with anomalies of 5.63°C and 6.56°C, respectively. The anomaly moderated slightly in spring, when only Rothera Station recorded the third-highest spring mean SAT (2.91°C above normal).

Similarly, the warm anomaly in Victoria Land peaked in winter, with all five stations in the region ranking among the top three highest on record; Manuela Station achieved a new record high (2.91°C above normal). The anomaly weakened in spring, though Marble Point and Cape Ross Stations still recorded the third-highest spring mean SATs (2.16°C and 1.44°C above normal, respectively).

In the Dome regions of East Antarctica, Princess Elizabeth Land, and Dronning Maud Land, the

warm anomaly was most pronounced in spring. Vostok, Davis, Zhongshan, and Mawson Stations each recorded their highest spring mean SATs on record, with anomalies of 3.28°C, 3.27°C, 3.30°C, and 3.39°C, respectively. Syowa and Novolazarevskaya Stations recorded the second-highest spring mean SATs, with anomalies of 2.98°C and 2.48°C.

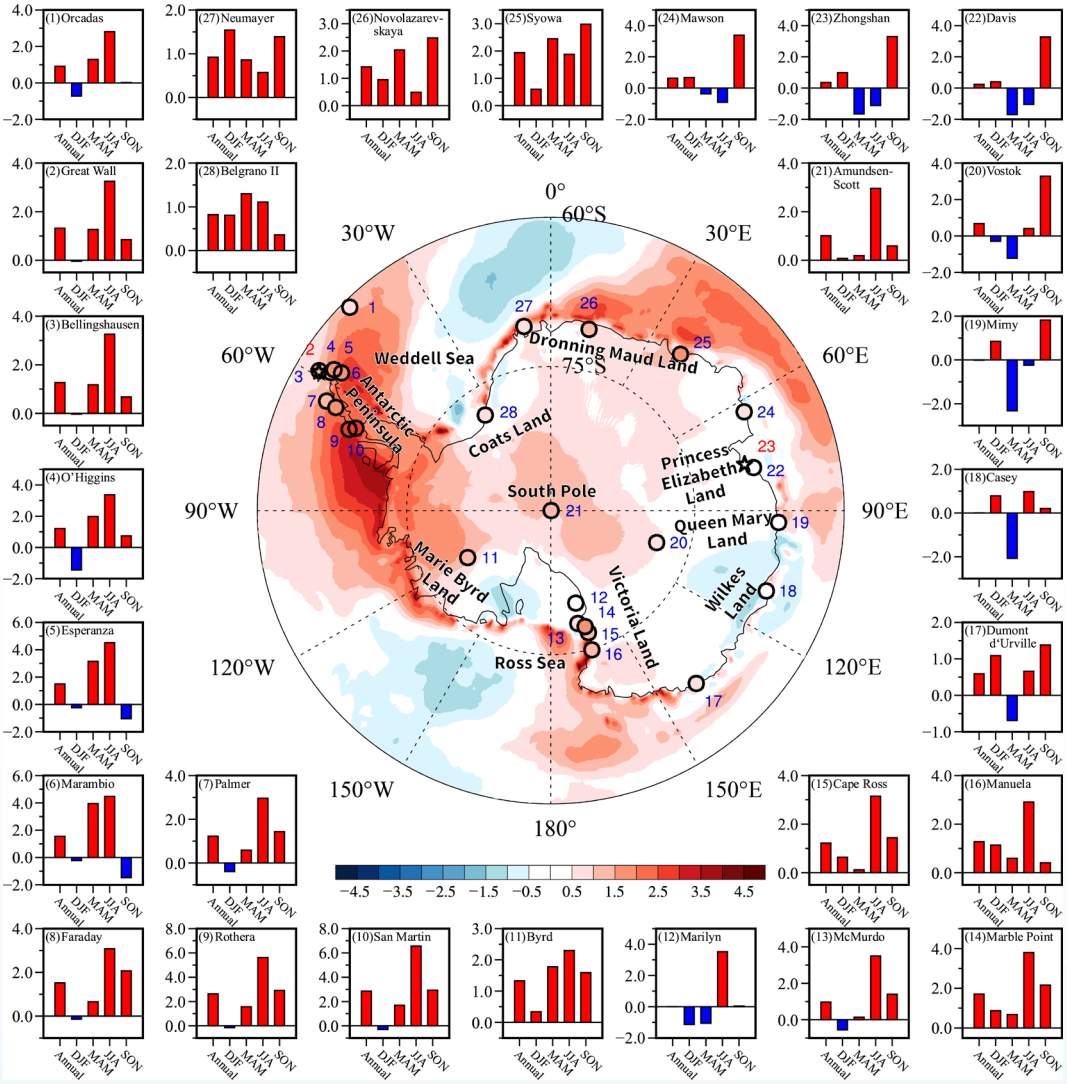

Figure 1.1 Spatial distribution of the 2025 annual mean surface air temperature (SAT) anomalies in Antarctica and the annual and seasonal mean SAT anomalies at various stations (unit: °C)

Globally, annual SAT exhibited a significant upward trend from 1979 to 2025, with a warming rate of 0.18°C per decade ($p < 0.01$; Figure 1.2). In parallel, warming over the Antarctic continent occurred at a slightly higher rate of 0.20°C per decade ($p < 0.05$), marginally exceeding the global average (Figure 1.2). Further analysis reveals warming trends across all seasons, albeit with substantial seasonal differences: summer and spring warmed most rapidly, at rates of 0.27°C and 0.35°C per decade, respectively ($p < 0.01$), while autumn and winter showed weaker, statistically insignificant trends of 0.03°C and 0.09°C per decade ($p > 0.1$).

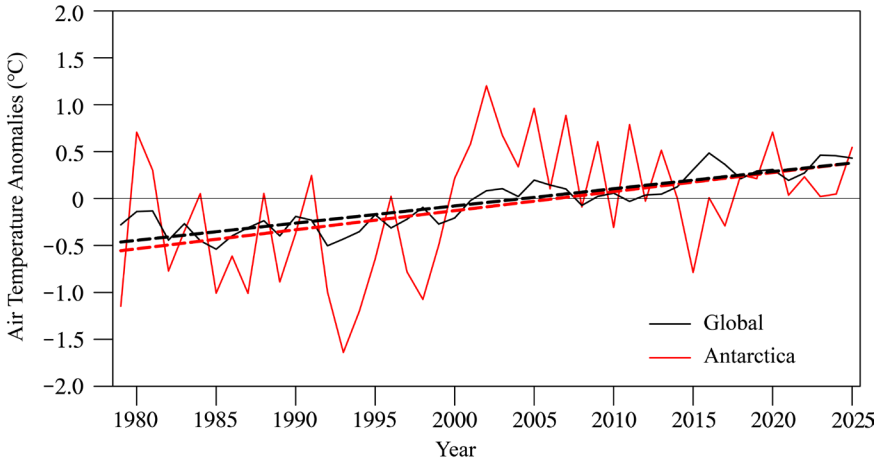

Figure 1.2 Time series of annual mean surface SAT anomalies averaged over Antarctic Continent (solid red line) and globally (solid black line) from 1979 to 2025, along with their trends (dashed lines) (unit: °C)

Although the overall SAT trend over Antarctica is comparable to the global average, certain regions exhibit markedly accelerated warming. The Antarctic Peninsula remains one of the fastest-warming areas

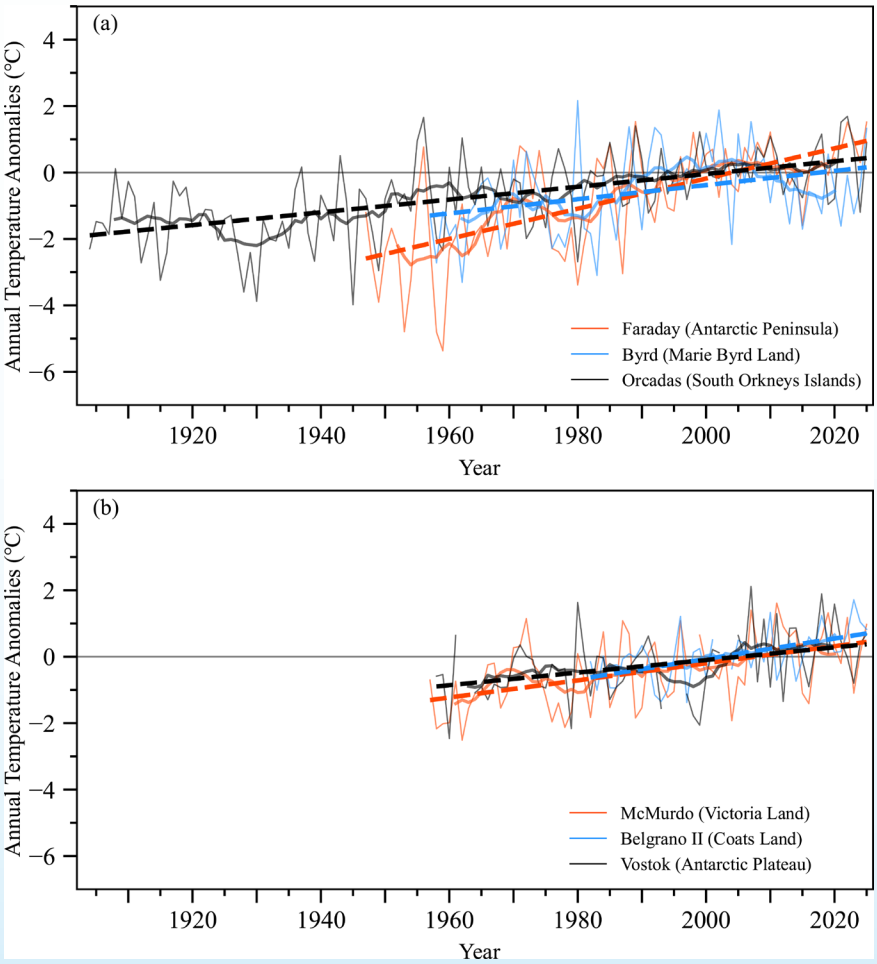

Figure 1.3 Time series of annual mean SAT anomalies at warming sites in the West Antarctic (a) and East Antarctic (b) regions. The thin solid line represents the annual mean SAT anomalies, the thick solid line represents the 11-year running average of annual mean SAT anomalies, and the dashed line indicates the trend in annual mean SAT anomalies

worldwide, with Faraday Station recording a rate of 0.45°C per decade (1947–2025; red line in Figure 1.3a). The South Orkney Islands, Marie Byrd Land, Victoria Land, Coats Land, and the Antarctic Dome regions also display upward trends, though at more moderate rates: 0.19°C per decade (1904–2025; black line in Figure 1.3a), 0.21°C per decade (1957–2025; blue line in Figure 1.3a), 0.26°C per decade (1957–2025; red line in Figure 1.3b), 0.31°C per decade (1982–2025; blue line in Figure 1.3b), and 0.19°C per decade (1958–2025; black line in Figure 1.3b), respectively. Elsewhere across the Antarctic continent, no significant long-term changes in annual SAT were observed.

Extreme Events

On 12 October 2025, a rare rainfall event was recorded at China's Zhongshan National Atmospheric Background Station in Antarctica. This event was associated with anomalous temperatures in the surrounding region, highlighting the significant impact of global warming on East Antarctica. Rainfall in Antarctica poses a serious threat to the local ecosystem, as freezing rain followed by ice formation can increase the risk of frostbite for native polar species, such as penguin chicks, potentially endangering their survival.

1.1.2 Arctic

This subsection systematically examines SAT changes in the Arctic, drawing on data from the Global Historical Climatology Network-Daily (GHCN-D), the Greenland weather observation dataset provided by the Danish Meteorological Institute, and the CMA-RA reanalysis product. All datasets have undergone strict quality control.

Results show that the annual mean SAT in the Arctic region in 2025 was –6.40°C, 1.14°C above the climatological normal. Seasonally, mean SAT values for boreal winter (December–February), spring (March–May), summer (June–August), and autumn (September–November) were –17.75°C, –9.37°C, 6.43°C, and –4.60°C, respectively. All seasons in 2025 were warmer than normal, with the most substantial anomalies occurring in winter and autumn (2.13°C and 1.78°C), and smaller anomalies in spring and summer (0.84°C and 0.15°C).

Spatially, most Arctic areas recorded SATs above the climatological normal in 2025, with the exception of Eastern Siberia, which experienced a below-average annual SAT (Figure 1.4). Among all Arctic observation stations, Thule (Greenland) and Ny-Alesund (Norway) registered the largest warming amplitudes, both 2.2°C above normal (Figure 1.4-5, 8). A prominent warm anomaly center existed around the Barents Sea, where Bodoe (Norway) and Teriberka (Russia) recorded their highest annual mean SAT on record (Figure 1.4-9, 13); Ny-Alesund recorded its second-highest (Figure 1.4-8); and Tromso (Norway) and Inari (Finland) recorded their third-highest (Figure 1.4-10, 12). The smallest warming amplitude was observed at Kotzebue (USA), with an anomaly of just 0.2°C (Figure 1.4-1).

Seasonally, the warm anomalies in winter and autumn of 2025 were more pronounced than those in spring and summer. In winter, Bettles (USA) recorded a mean SAT 4.7°C above normal—the largest winter anomaly across the Arctic (Figure 1.4-3). All stations in the USA and Canada reported winter mean SATs more than 3°C above the climatological baseline. In spring 2025, Thule (Greenland) exhibited the largest warming amplitude, with a spring mean SAT 2.9°C above normal, marking the second-highest on record

(Figure 1.4-5). Spring mean SATs at other stations remained within 1.5°C above normal, although Kotzebue (USA), Paulatuk (Canada), and Daneborg (Greenland) showed cold anomalies in winter (Figure 1.4-1, 4, and 6). In summer 2025, a distinct warm anomaly appeared along the coasts of the Barents and Kara Seas. Mare-Sale and Novy Port (Russia) experienced the largest summer anomalies, both 2.6°C (Figure 1.4-14, 15). Jan Mayen (Norway) recorded its highest summer mean SAT on record (Figure 1.4-7), while Ny-Alesund (Norway) and Novy Port (Russia) registered their second-highest (Figure 1.4-8, 15). Over the North American continent, the summer warm anomaly was weak, and slight cold anomalies occurred at Thule and Daneborg in Greenland (Figure 1.4-5, 6). In autumn 2025, a basin-wide warm anomaly blanketed the Arctic. Paulatuk (Canada) recorded an autumn mean SAT 3.9°C above normal—the highest on record (Figure 1.4-4), and Teriberka (Russia) logged its second-highest autumn mean SAT (Figure 1.4-13).

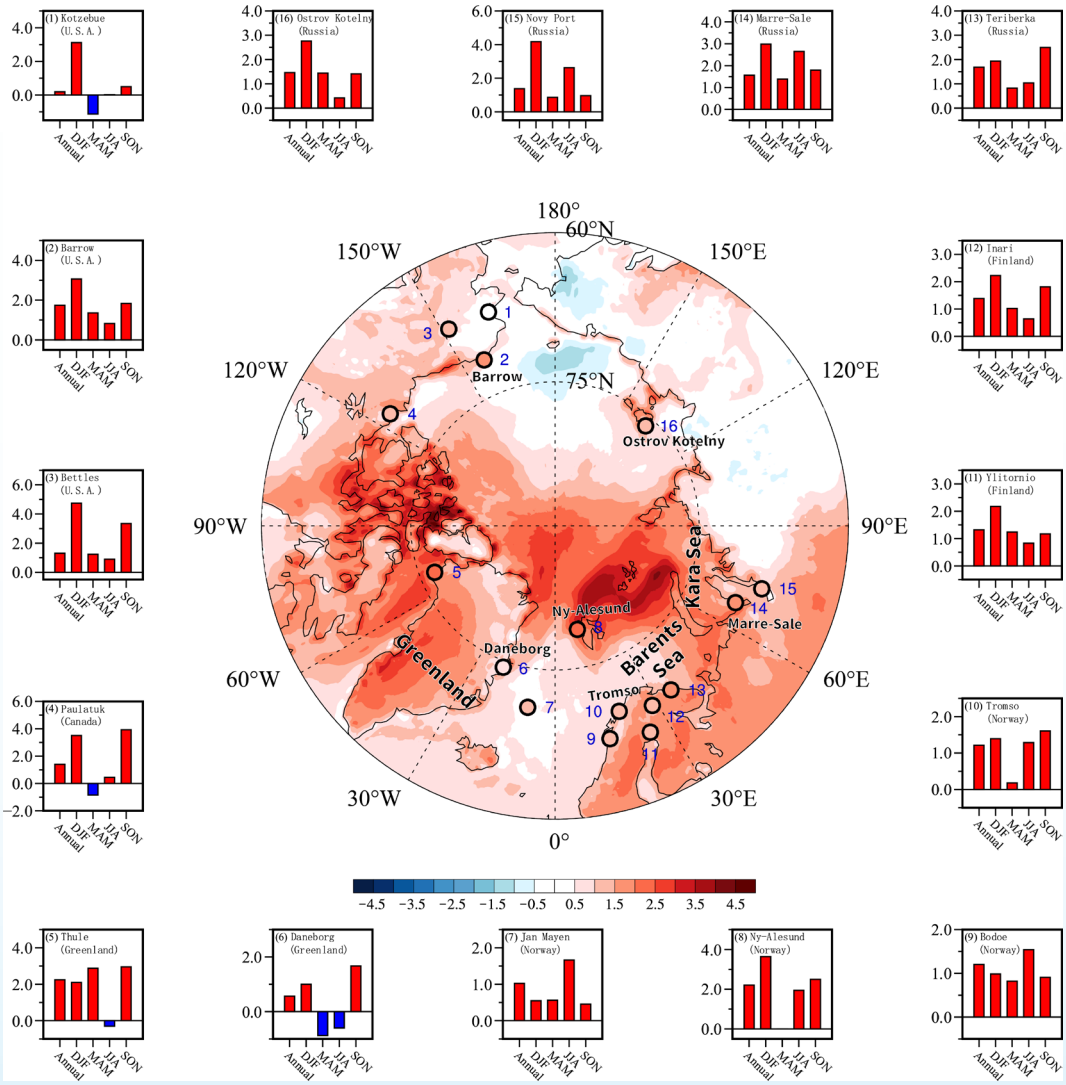

Figure 1.4 Spatial distribution of the 2025 annual mean SAT anomalies in Arctic and the annual and seasonal mean SAT anomalies at various stations (unit: °C)

Amidst global warming, the Arctic region exhibited a rapid upward trend in annual mean SAT during 1979–2025 (Figure 1.5), at a rate of 0.52°C per decade ($p < 0.01$)—2.9 times the global average—underscoring the Arctic's heightened sensitivity to climate change. Seasonally, significant warming trends were observed in all seasons, with the strongest rates in autumn and winter (0.75°C and 0.56°C per decade,

respectively), followed by spring (0.49°C per decade) and summer (0.31°C per decade).

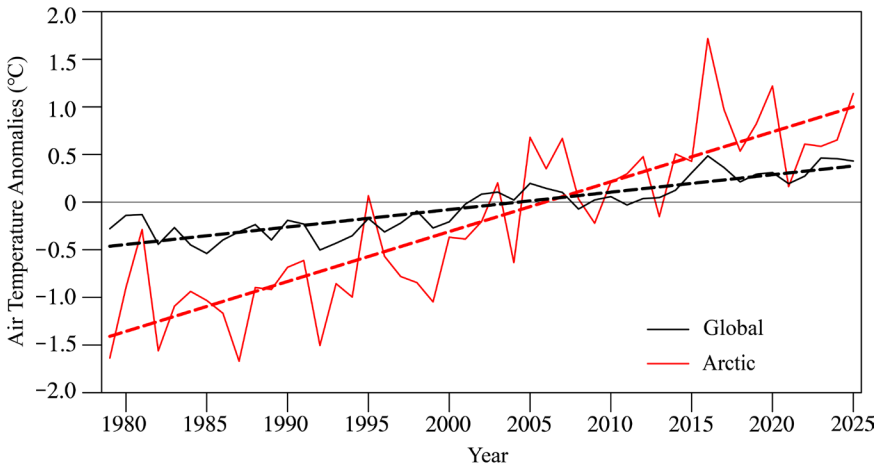

Figure 1.5 Time series of annual mean SAT anomalies averaged over Arctic (solid red line) and globally (solid black line) from 1979 to 2025, along with their trends (dashed lines) (unit: °C)

This rapid Arctic warming is particularly evident over the Arctic Ocean. Although warming over land

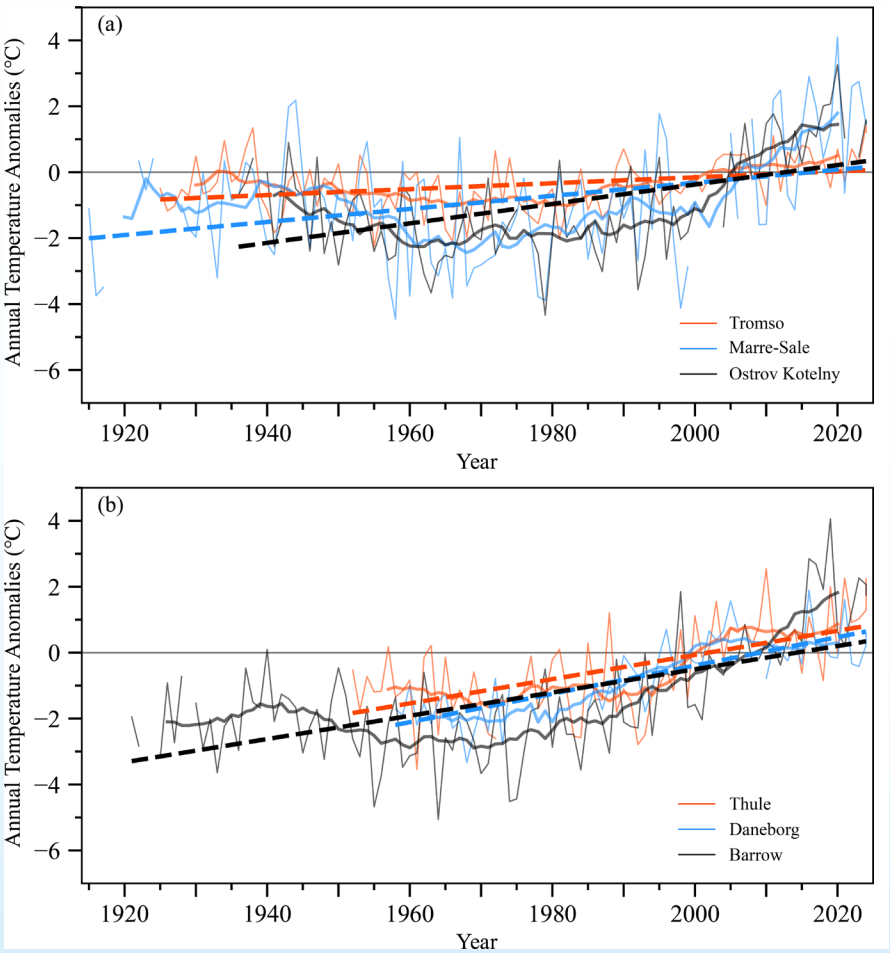

Figure 1.6 Time series of annual mean SAT anomalies at warming sites in the Arctic regions of Eurasia (a) and North America (b). The thin solid line represents the annual mean SAT anomalies, the thick solid line represents the 11-year running average of annual mean SAT anomalies, and the dashed line indicates the trend in annual mean SAT anomalies

areas is comparatively slower, it still substantially exceeds the global mean. Since the onset of instrumental records, all Arctic stations have displayed significant warming trends, with acceleration since the 1980s (Figure 1.6). During 1981–2025, Barrow (Alaska) warmed at 1.07°C per decade; Mare-Sale and Kotelnyi (Siberia) at 0.83°C and 0.96°C per decade, respectively; Thule (Greenland) at 0.68°C per decade; while Daneborg and Tromso (North Atlantic sector) exhibited relatively slower rates of 0.43°C and 0.36°C per decade.

Extreme Events

In May 2025, Iceland and Greenland saw record-breaking heatwaves, with temperatures in some regions being more than 10°C above the average. The Ittoqqortoormiit station in Greenland saw temperatures reach 14.3°C on May 19, which is more than 13°C above the May average daily maximum temperature of 0.8°C. Driven by climate warming, the melting of the Greenland ice sheet in mid-May was about 17 times higher than the average for this period.

1.2 Sea Surface Temperature

This section utilizes the Operational Sea Surface Temperature and Sea Ice Analysis (OSTIA) dataset, a global high-resolution sea surface temperature (SST) and sea ice cover product released by the UK Met Office. We analyze SST anomalies using the 1991–2020 climatological mean as the baseline.

1.2.1 Southern Ocean

In March 2025, Antarctic coastal sea ice was at its annual melting peak, with residual ice areas in the Weddell Sea and Ross Sea becoming the main sea ice coverage regions. Sea surface temperatures across the entire Southern Ocean showed overall warming compared to the long-term average, with small-scale cold anomalies appearing only in the western Atlantic sector and eastern Pacific sector, forming a distinct dipole-type anomaly distribution (Figure 1.7a). Compared to the same period in 2024, March 2025 Southern Ocean sea surface temperatures were still dominated by warm anomalies, but the intensity and spatial extent of cold anomalies were more pronounced compared to climatological normal values (Figure 1.7c), reflecting differences in interannual sea surface temperature anomaly structures.

In September 2025, Southern Ocean sea ice coverage expanded to around 60°S. Compared to the climatological baseline period, sea surface temperatures across the entire Southern Ocean still showed a warming trend (Figure 1.7b). However, interannual comparison reveals that the sea surface temperature anomaly pattern in September 2025 underwent significant changes, characterized mainly by cold anomalies (Figure 1.7d). The cold anomalies were primarily concentrated in the central Pacific sector, Indian Ocean sector, and eastern Atlantic sector, while the western Atlantic sector and western Indian Ocean sector still maintained warm anomalies. This regional warm-cold contrast may be closely related to the non-uniform nature of spring sea ice freezing processes in different Southern Ocean sectors and spatial differences in surface cooling intensity.

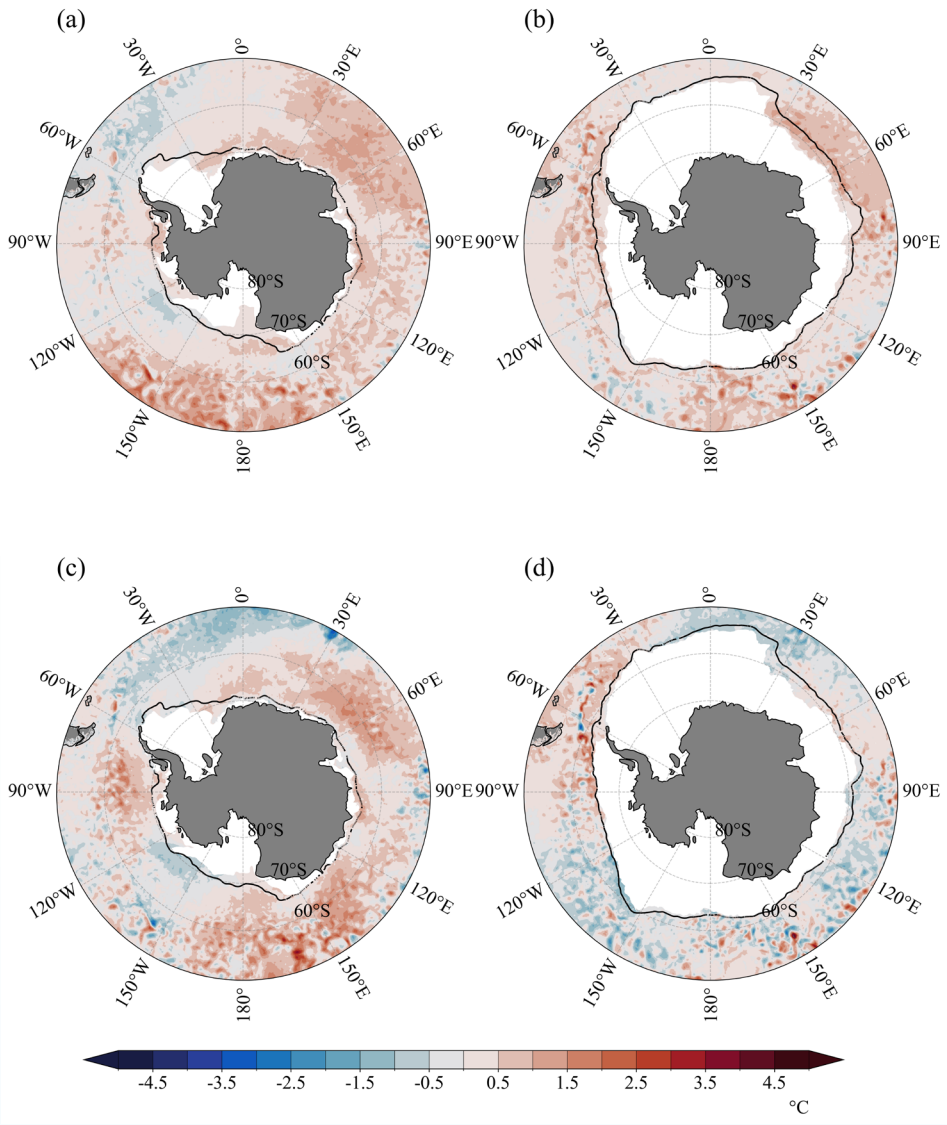

Figure 1.7 SST Anomaly Distribution in the Southern Ocean, March and September 2025
(a) Sea Surface Temperature Anomaly (SST Anomaly) in the Southern Ocean, March 2025 (Unit: ℃); (b) SST Anomaly in the Southern Ocean, September 2024 (Unit: ℃); (c) SST Anomaly in the Southern Ocean, March 2025 Relative to March 2024 (Unit: ℃); (d) SST Anomaly in the Southern Ocean, September 2025 Relative to September 2024 (Unit: ℃). In all panels, white areas and black solid lines indicate the climatological mean sea ice extent and marginal ice zone position for the respective months, respectively

1.2.2 Arctic Ocean

Compared to long-term climatological conditions, Arctic Ocean sea surface temperatures in March 2025 exhibited an overall warming characteristic, with warm anomalies being most pronounced in the Atlantic sector of the Arctic Ocean, particularly in the Bering Strait and Barents Sea (Figure 1.8a). Interannual comparison reveals that Arctic Ocean sea surface temperatures in March 2025 were overall higher than those in the same period of 2024, with the warming signal being particularly strong in the Chukchi Sea and Beaufort Sea in the Pacific sector (Figure 1.8c), which corresponds to changes in the sea ice retreat process in

the Pacific sector during this period.

In September 2025, Arctic Ocean sea surface temperatures showed pronounced warming relative to the long-term average, with only the Chukchi Sea and the southern coastal waters of the Beaufort Sea maintaining cold anomaly characteristics (Figure 1.8b). In comparison with the same period in 2024, September 2025 sea surface temperature anomalies demonstrated significant regional disparities: the Kara Sea, Bering Sea, and Greenland Sea were primarily characterized by persistent warm anomalies, while the Beaufort Sea, Laptev Sea, and the Barents Sea exhibited alternating warm and cold patterns. This regional heterogeneous distribution pattern reflects the phase differences in sea ice melting processes across different sectors, as well as the regulatory effects of atmospheric circulation anomalies on regional sea surface temperatures.

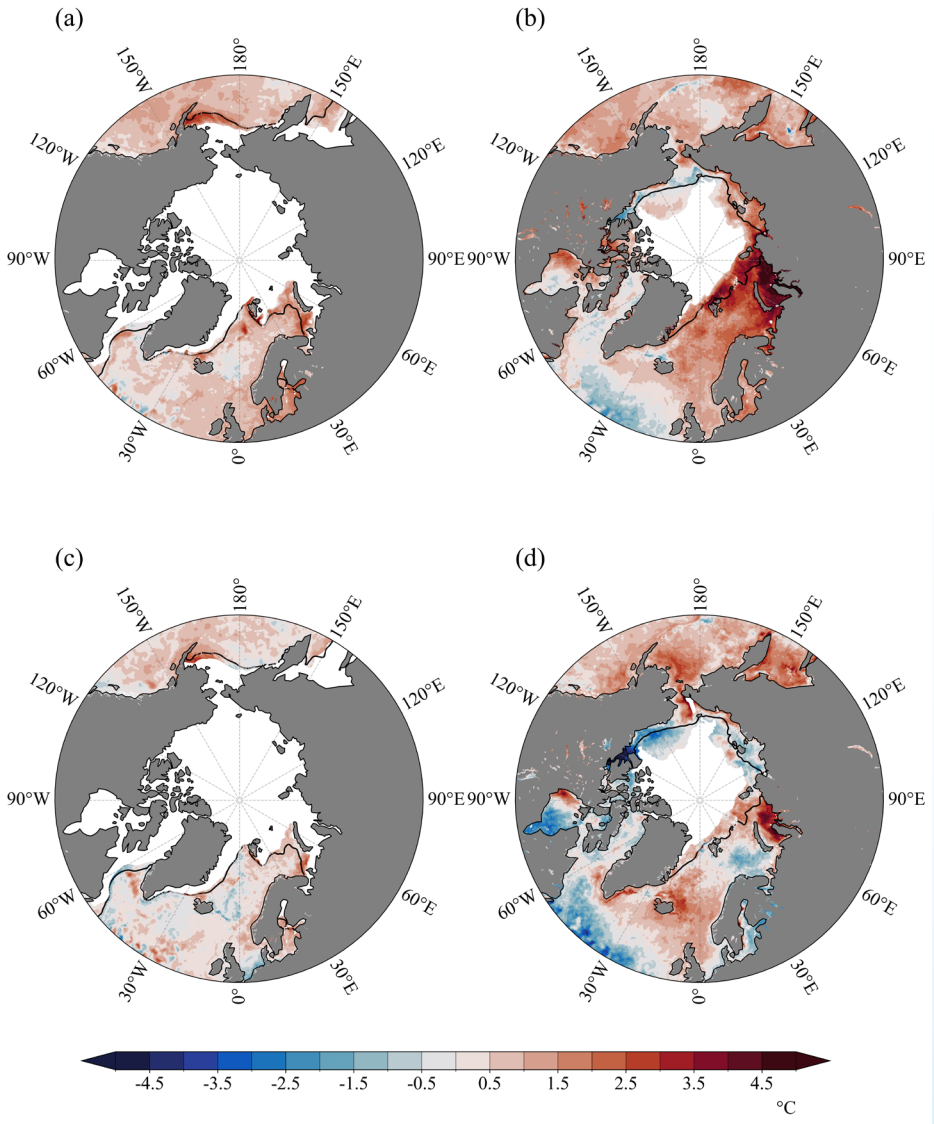

Figure 1.8 Arctic Ocean SST Anomaly Distribution, March and September 2025
(a) Sea Surface Temperature Anomaly (SST Anomaly) in the Arctic Ocean, March 2025 (Unit: ℃); (b) SST Anomaly in the Arctic Ocean, September 2025 (Unit: ℃); (c) SST Anomaly in the Arctic Ocean, March 2025 Relative to March 2024 (Unit: ℃); (d) SST Anomaly in the Arctic Ocean, September 2025 Relative to September 2024 (Unit: ℃). In all panels, white areas and black solid lines denote the climatological mean sea ice extent and marginal ice edge position for the corresponding months, respectively

Extreme Events

In August 2025, a relatively strong sea surface temperature extreme event occurred in the Arctic region. Arctic Ocean sea surface temperatures reached the second highest on record that month (second only to August 2007), approximately 0.8℃ above the climatological average. Among these, the Kara Sea experienced the most significant warming, with sea surface temperatures reaching a historical maximum for the region, approximately 5℃ above the climatological average.

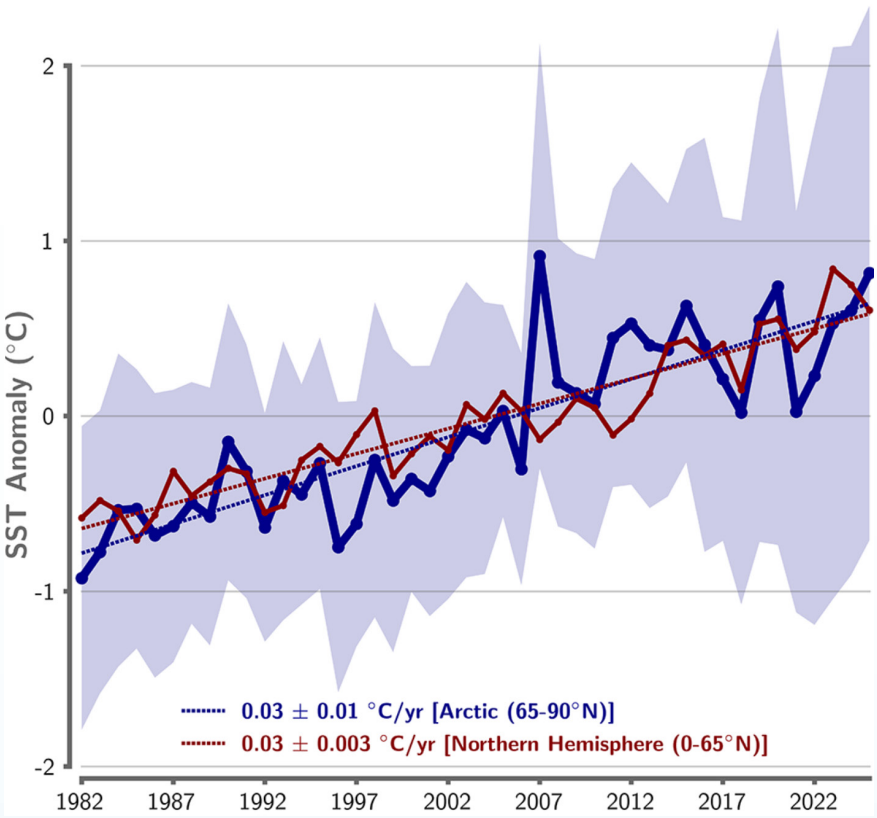

Arctic and Northern Hemisphere August Sea Surface Temperature (SST) Anomaly Series (1982–2025): Arctic Ocean Domain (65°N and north; blue line) and Northern Hemisphere (0–65°N; red line) with linear trend lines (dashed lines) (Source: Arctic Report Card 2025)

1.3 Air pressure

Changes in the air pressure field are one of the key linkages between the polar regions and the global climate. This section analyzes the spatial anomaly characteristics of the air pressure fields in the Arctic and Antarctic in 2025, as well as important circulation phenomenons such as the polar vortex and atmospheric oscillations. The Arctic polar vortex index is sourced from the National Climate Center, and the oscillation indices are calculated with CMA-RA reanalysis dataset.

1.3.1 Antarctic

In the summer of 2025, the 500hPa geopotential height anomaly field over the Antarctic continent displayed weak positive anomalies. There was a negative anomaly center extending from the South Indian Ocean to south of Australia, and a strong positive anomaly center above the water north of the Ross Sea, overall exhibiting the characteristics of the negative phase of the Southern Annular Mode (Fig. 1.9a). In winter, the circumpolar geopotential height anomaly field resembled an approximate three-wave pattern, with the most prominent negative anomaly center near the Amundsen Sea. Over the Antarctic continent, positive and negative anomalies alternated without a large-scale, uniform anomaly center, and the circulation characteristics were close to the neutral phase of the Southern Annular Mode (Fig. 1.9b). The distributions of the summer and winter sea level pressure anomaly fields were highly consistent with those of the 500hPa geopotential height anomaly fields, reflecting typical barotropic structural characteristics (Fig. 1.9c, d)

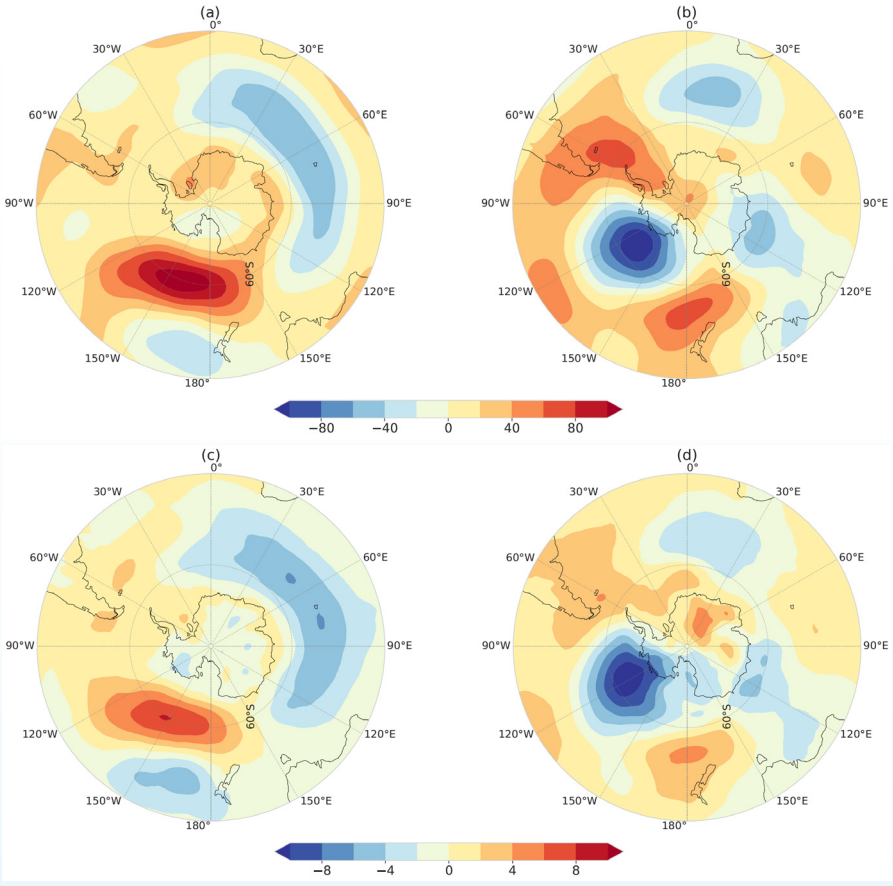

Fig. 1.9 The 500hPa geopotential height anomaly fields in the Southern Hemisphere in (a) summer (Dec–Feb) and (b) winter (Jun–Aug) of 2025 (unit: gpm), and sea level pressure anomaly fields in (c) summer and (d) winter (unit: hPa) of 2025

In 2024, the standardized Antarctic Oscillation (AAO) index recorded its highest positive value (since 1979) in summer, and its 5th strongest negative value (since 1979) in winter. This seasonal difference weakened in 2025. The 2025 summer AAO index shifted to a negative value (-1.00), the 11th strongest negative value between 1979 and 2025; the winter AAO index turned into a mild positive value (0.72), and the annual mean AAO index was 0.16, such a value near zero corresponding to neutral AAO phase characteristics (Fig. 1.10). From 1979 to 2025, the trend values of the AAO index for summer, winter, and

the whole year were 0.39/decade, -0.01/decade, and 0.20/decade, respectively. Both the summer and annual trends reached the 0.05 significance level, while the winter trend was not statistically significant.

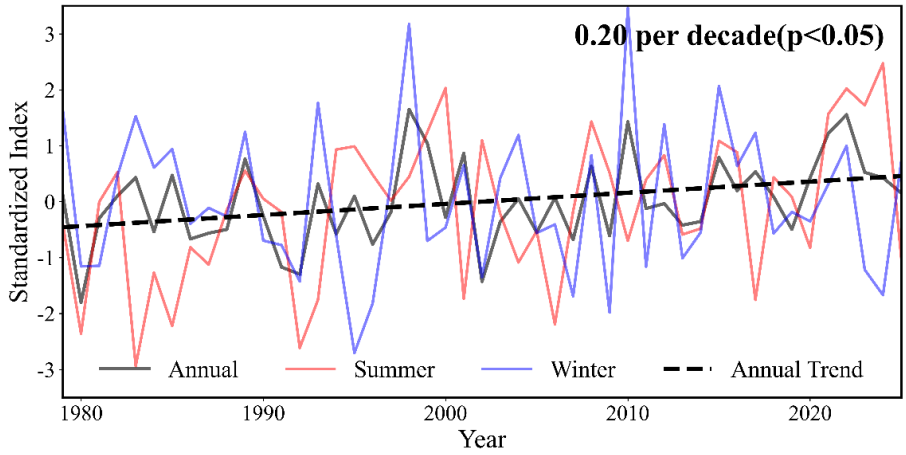

Fig. 1.10 Standardized Antarctic Oscillation (AAO) index, 1979–2025

1.3.2 Arctic

As shown in Fig.1.11, in the boreal winter of 2025, the 500hPa height field exhibits several scattered positive anomaly centers over the Arctic Ocean and northern Eurasia, while widespread and closed negative

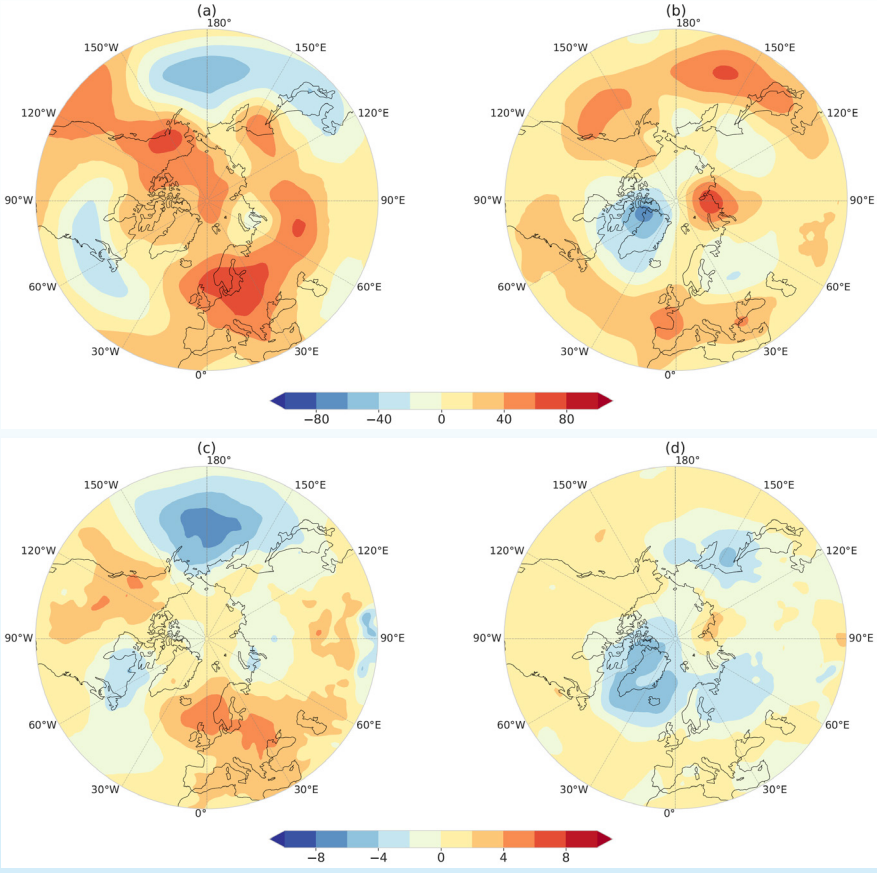

Fig. 1.11 The 500hPa geopotential height anomaly fields in the Northern Hemisphere in (a) summer (Dec–Feb) and (b) winter (Jun–Aug) of 2025 (unit: gpm), and sea level pressure anomaly fields in (c) summer and (d) winter (unit: hPa) of 2025

anomaly centers are found near the North Pacific-Bering Strait and the North American continent-North Atlantic; in the boreal summer of 2025, the 500hPa height field is mostly dominated by negative anomalies over the Arctic Ocean, with the center located over Greenland, whereas the circum-Arctic region outside this negative center is basically dominated by positive height anomalies. Overall, the 500hPa height field in the Arctic region exhibits characteristics approximating the positive phase of the Arctic Oscillation in summer, while it shows no obvious Arctic Oscillation phase characteristics in winter.

As shown in Fig. 1.12, the standardized index of the Northern Hemisphere (NH) polar vortex area in 2025 was -2.228 (winter) / -0.787 (summer) / -1.857 (annual mean), with changes of -1.936 (winter) / 0.853 (summer) / 0.630 (annual mean) respectively compared to 2024. It can be seen that the NH polar vortex area index decreased significantly in the winter of 2025, setting a new record low for the winter NH polar vortex area index during the period 1979–2025, while the polar vortex area index increased in summer and on an annual mean basis. The standardized index values for the NH polar vortex intensity in 2025 were -1.938 (winter) / -0.503 (summer) / -1.446 (annual mean), with changes of -0.997 (winter) / 0.005 (summer) / 0.245 (annual mean) respectively compared to 2024. The polar vortex deepened significantly in the winter of 2025; in terms of absolute magnitude, the polar vortex intensity in the winter of 2025 was second only to 2010. The changes in polar vortex area/intensity in winter, summer, and the annual mean in 2025 did not alter the significant negative trend of the NH polar vortex area/intensity index since 1979.

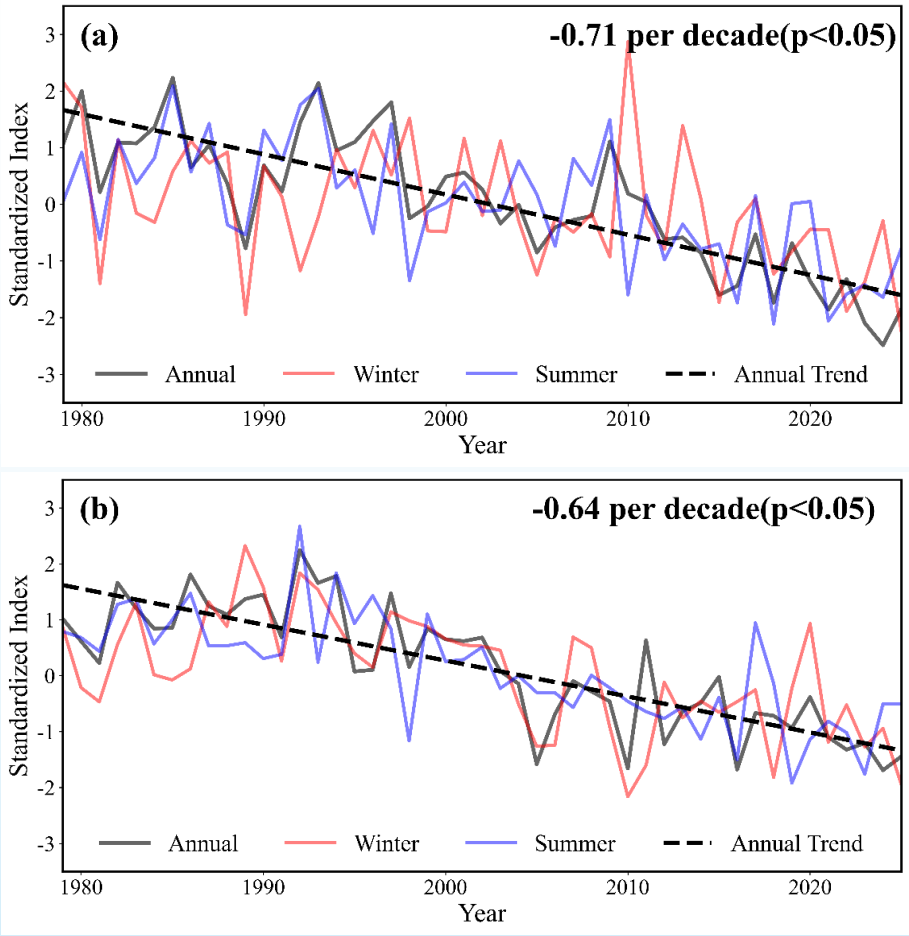

Fig. 1.12 Standardized indices of (a) Northern Hemisphere polar vortex area and (b) Northern Hemisphere polar vortex intensity from 1979 to 2025

The standardized Arctic Oscillation index in 2025 was 0.06 (winter) / 1.08 (summer) / 0.58 (annual mean), where the summer showed a strong positive anomaly, as shown in Fig.1.13.

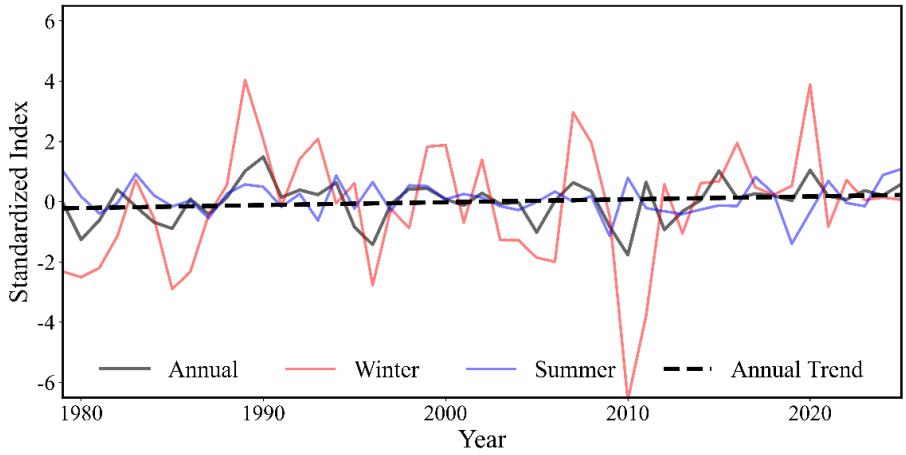

Fig. 1.13 Standardized Arctic Oscillation (AO) index from 1979 to 2025

Chapter 2 Sea Ice

The data utilized in this chapter include the sea ice extent product (G02135_v4.0) from the National Snow and Ice Data Center (NSIDC) in the USA, covering the period 1979-2025, with climatology defined as the average over 1991-2020. Additionally, sea ice concentration products derived from China's Fengyun series satellites—provided by Sun Yat-sen University and Ocean University of China (OUC)—as well as sea ice surface melt onset/freeze onset datasets from the National Aeronautics and Space Administration (NASA) in the USA and OUC, are also employed.

2.1 Sea Ice Extent

2.1.1 Antarctic

Antarctic sea ice extent exhibits pronounced seasonal variability (Fig. 2.1a). Sea ice grows roughly from March to September each year, while melting occurs from October to February of the following year. The annual minimum sea ice extent typically appears in late February to early March. On 1 March 2025, the Antarctic sea ice extent reached its annual minimum of 1.96×10^6 km^2, ranking as the third lowest on record, behind the minima recorded in 2023 (21 February, 1.85×10^6 km^2) and 2022 (25 February, 1.95×10^6 km^2). The annual maximum Antarctic sea ice extent in 2025 was 17.85×10^6 km^2, also the third lowest in history, following 2023 (17.11×10^6 km^2) and 2024 (17.28×10^6 km^2). Overall, Antarctic sea ice extent in 2025 was abnormally low, with the annual mean being the third lowest, surpassed only by those in 2023 and 2024.

In terms of the long-term trend, Antarctic sea ice extent during 1979-2025 shows a pattern of slow increase followed by rapid decrease. Since 1979, the overall rate of decrease in Antarctic sea ice extent has been 7.15×10^4 km^2 per decade (Fig. 2.1b).

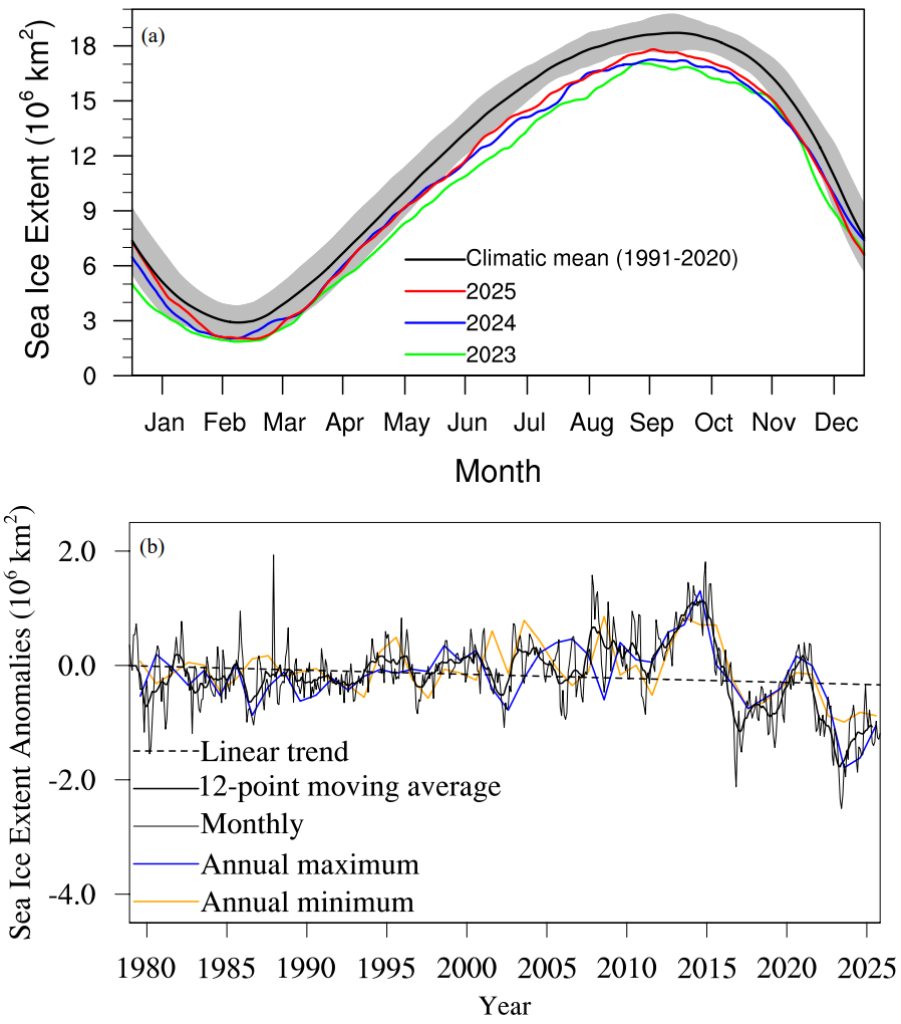

Fig. 2.1 (a) Climatological monthly mean Antarctic sea ice extent with ±2 standard deviations (gray shading), along with monthly Antarctic sea ice extent for 2023, 2024, and 2025; (b) Time series of annual minimum (orange) and maximum (blue) Antarctic sea ice extent anomalies, monthly mean Antarctic sea ice extent anomalies (thin black line), their 12−month running mean (thick black solid line), and linear trend for 1979−2025 (unit: 10^6 km^2)

2.1.2 Arctic

Arctic sea ice extent also displays distinct seasonal variability (Fig. 2.2a). Sea ice grows from late September to March of the following year, and melts from April to mid-September. The annual minimum sea ice extent usually occurs in mid-September. Although the annual minimum Arctic sea ice extent in 2025 ranked the 10th lowest, the annual maximum reached a 47-year low of 14.35×10^6 km^2 (on 21 March). Furthermore, the monthly mean Arctic sea ice extent during several winter months broke historical records, resulting in an extremely low annual mean Arctic sea ice extent in 2025, which set a new record minimum of 10.13×10^6 km^2.

Regarding the long-term trend (Fig. 2.2b), since 1979, Arctic sea ice extent has decreased at an overall

rate of 5.13×10^5 km^2 per decade, with the annual minimum extent decreasing at a rate of 7.65×10^5 km^2 per decade and the annual maximum extent decreasing at a rate of 3.91×10^5 km^2 per decade.

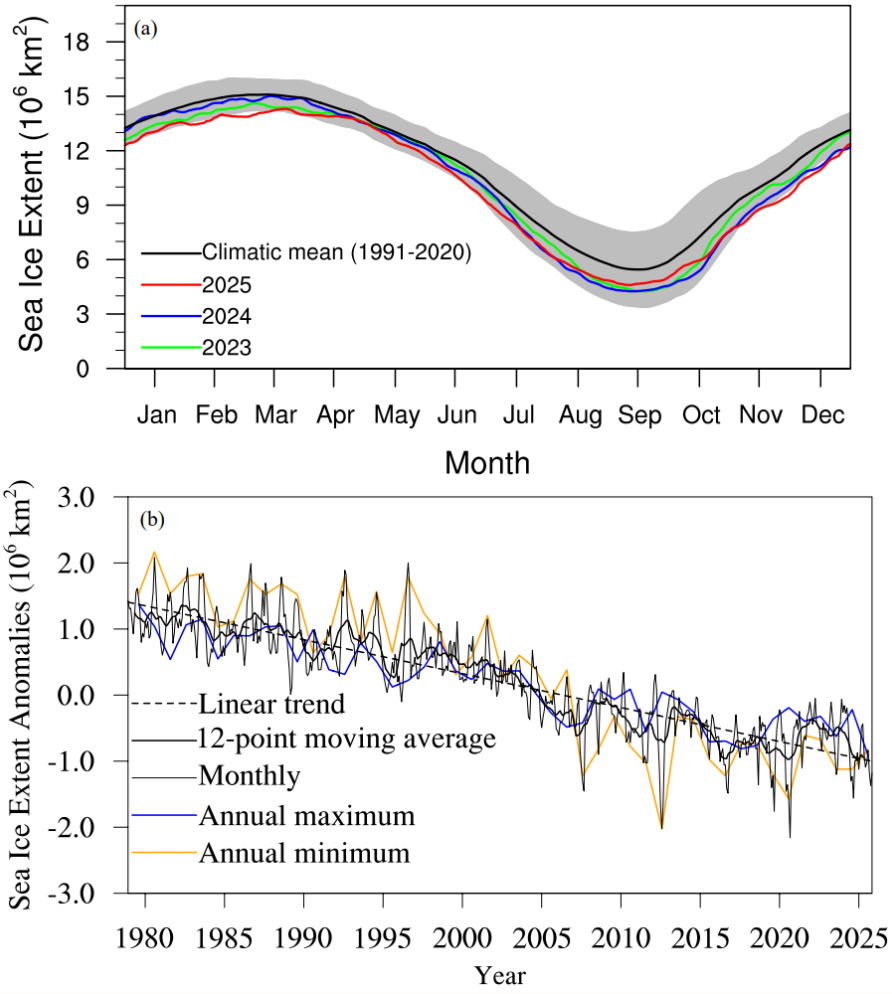

Fig. 2.2 (a) Climatological monthly mean Arctic sea ice extent with ±2 standard deviations (gray shading), along with monthly Arctic sea ice extent for 2023, 2024, and 2025; (b) Time series of annual minimum (orange) and maximum (blue) Arctic sea ice extent anomalies, monthly mean Arctic sea ice extent anomalies (thin black line), their 12−month running mean (thick black solid line), and linear trend for 1979−2025 (unit: 10^6 km^2)

2.2 Sea ice concentration

2.2.1 Antarctica

Figure 2.3 presents the monthly Antarctic sea ice concentration (SIC) mean and corresponding anomalies for February and September 2025, relative to the average 2012-2025. Overall, Antarctic SIC in February was lower than the climatological average, with sea ice primarily distributed in the Weddell Sea, Amundsen Sea, and Ross Sea sectors of West Antarctica, while relatively limited coverage was observed along the East Antarctic coast. The Ross Sea exhibited notably higher SIC compared to the climatological

mean, whereas most other regions showed negative anomalies. It is worth noting that SIC in the western Weddell Sea was slightly above the climatological average, while the eastern Weddell Sea showed a pronounced decrease. In September, sea ice extensively surrounded the Antarctic continent, with a broader extent observed in West Antarctica. Compared to the climatological mean, significant variations in SIC were observed along the marginal ice zone, with regions of increase slightly exceeding those of decrease. Positive anomalies were mainly identified in the Weddell Sea and Ross Sea, whereas negative anomalies dominated in the Bellingshausen Sea and the western Indian Ocean sector. In contrast, the eastern Indian Ocean sector exhibited rather complex spatial variability, without a coherent changing pattern.

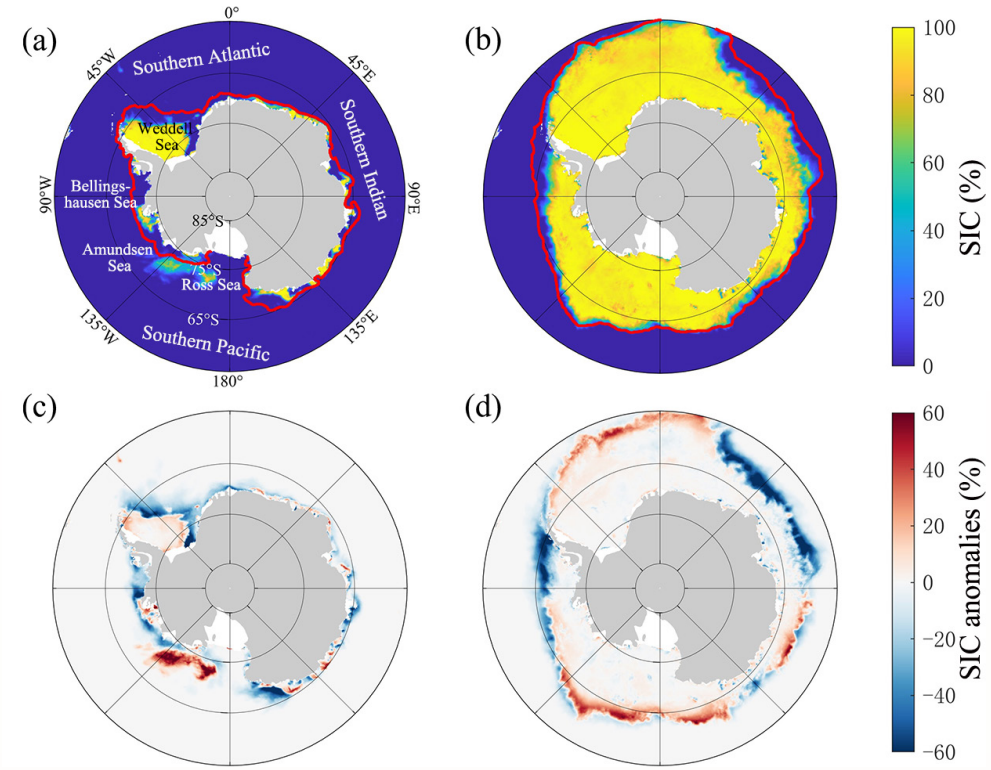

Fig. 2.3. The SIC monthly mean based on the Fengyun series meteorological satellite imagery for Antarctica in (a) February and (b) September; and its anomalies (relative to 2012–2025, unit: %) in (c) February and (d) September. The red solid line indicates the average sea ice extent during 2012–2025

2.2.2 Arctic

Figure 2.4 illustrates the monthly Arctic SIC mean and corresponding anomalies for March and September 2025. In March 2025, SIC over the central Arctic Ocean was generally consistent with the 2011-2025 climatological mean, while more pronounced anomalies were observed in the marginal ice zones. Increased SIC was evident in regions such as the Greenland Sea, whereas the Bering Sea exhibited complex spatial variability, with positive anomalies in the northern sector and negative anomalies in the southern sector. In the Sea of Okhotsk, SIC was predominantly below the climatological mean, although localized increases were observed in the western bay area. In September 2025, reductions in SIC were mainly distributed in the Beaufort Sea, the Canadian Arctic Archipelago, the Greenland Sea, and the Barents Sea. In contrast, regions of increased SIC were primarily concentrated in the high-latitude areas of the Laptev Sea and the East Siberian Sea.

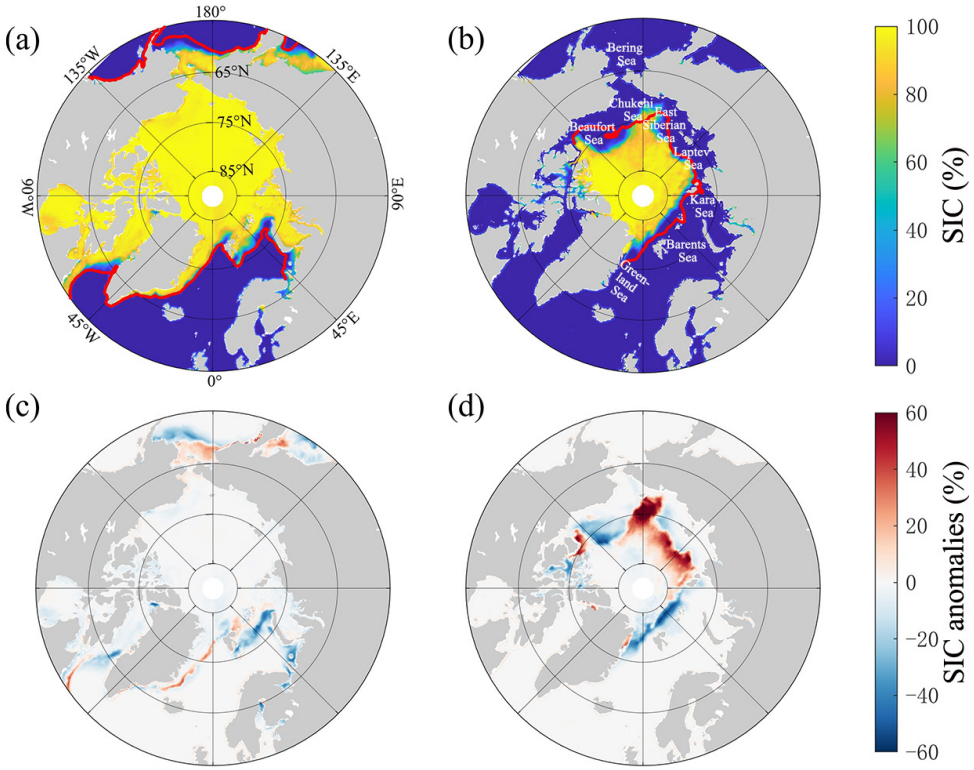

Fig. 2.4 The SIC monthly mean based on the Fengyun series meteorological satellite imagery for Arctic in (a) March and (b) September; and its anomalies (relative to 2012–2025, unit: %) in (c) March and (d) September. The red solid line indicates the average sea ice extent during 2012–2025

2.3 Sea Ice Melt Season

The onset of sea ice melt and freeze marks the beginning and end of the sea ice melt season. The melt onset (MO) is defined as the first day of continuous sea ice melting during summer, while the freeze onset (FO) is the first day when new ice begins to form in open water and the bare or lightly snow-covered ice surface undergoes continuous refreezing. The number of days between the MO and FO is the sea ice melt season length.

The Arctic sea ice surface MO spans from late March in the ice-margin areas to June in the central Arctic (Fig. 2.5a). Compared to the 2011-2025 average, the 2025 MO anomalies show a spatial inconsistency, with a general pattern of delayed MO in the central Arctic and earlier MO in the marginal sea ice regions. In the Laptev Sea, the Sea of Okhotsk, and the Hudson Bay region, MO shows a significant advancing trend. In stark contrast, in the marginal seas such as the Eurasian side of the central Arctic, the Beaufort Sea, the Chukchi Sea, the Kara Sea, and Baffin Bay, MO is significantly later than the multi-year average, with positive anomalies exceeding 20 days in some areas (Fig. 2.5c). In 2025, the mean date of MO in the regions north of 70°N was recorded as the 158th day, which is merely 1.3 days earlier than the average observed over the period from 2011 to 2025. The SMMR-SSM/I-SSMIS data published by NASA indicate that the MO in the Arctic exhibited an advancing trend from 1979 to 2022, with a rate of -1.47 d per decade. However, during the operational period of the FY-3B/3D satellites, both datasets revealed a delaying trend in the MO. Specifically, the MWRI data from 2011 to 2025 demonstrate that the MO was delayed at a rate of 3.6 d per

decade (Fig. 2.6a).

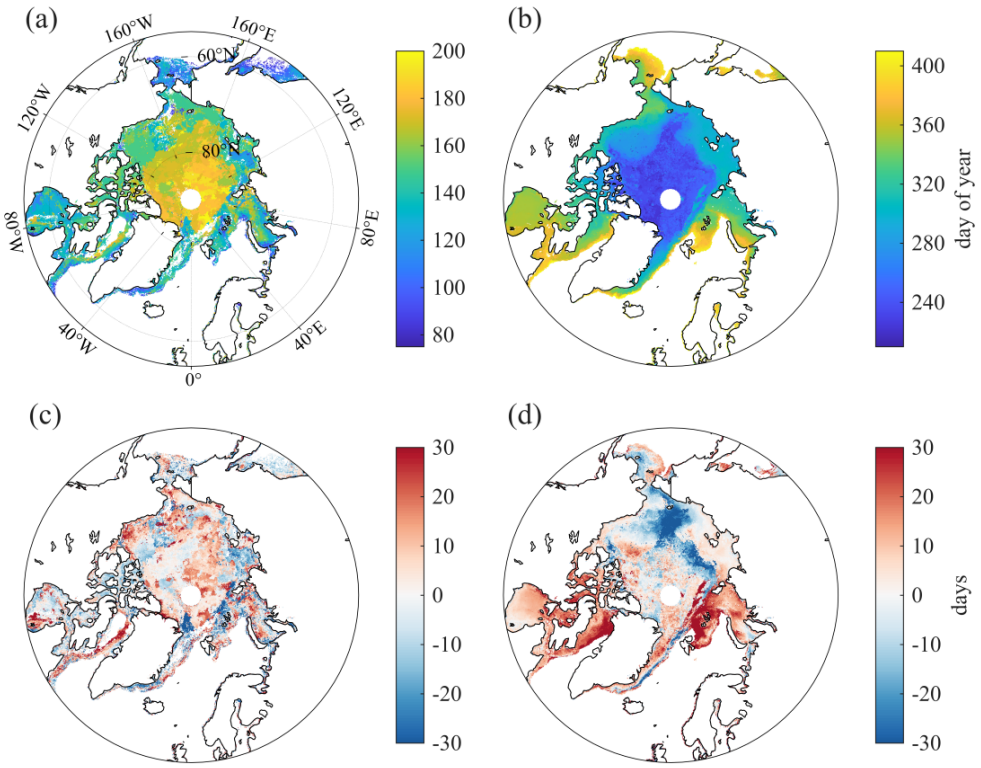

Figure 2.5 (a) Melt onset and (b) Freeze onset of 2025. (c) Melt onset and (d) Freeze onset anomalies of 2025

The Arctic sea ice surface FO spans from August in the central Arctic to January of the following year in the marginal sea ice region (Fig. 2.5b). Compared to the 2011-2025 average, the 2025 FO is characterized by earlier dates on the Pacific sector side, particularly in the northern East Siberian Sea and the Chukchi Sea, where local anomalies exceed 20 days earlier than the multi-year average, which is generally consistent with the regions displaying significant positive anomalies in September sea ice concentration (Fig. 2.4). In the central Arctic and the remaining marginal seas, the FO is predominantly delayed. In 2025, the average FO in regions north of 70°N was recorded as the 284th day, which is 5.2 days later than the average from 2011 to 2025. Data from the FY-3B/3D satellites show that during the period from 2011 to 2025, the FO exhibited a delaying trend at a rate of 5.1 d per decade (Fig. 2.6b).

The length of the sea ice melt season in the Arctic north of 70°N shows a lengthening trend in 1979-2022, with a rate of 6.3 d per decade. However, from 2011 to 2025, a slight shortening trend was observed, with a rate of 0.1 d per decade (Fig. 2.6c). As both MO and FO are delayed during this period, the trend in the length of the melt season is relatively weak.

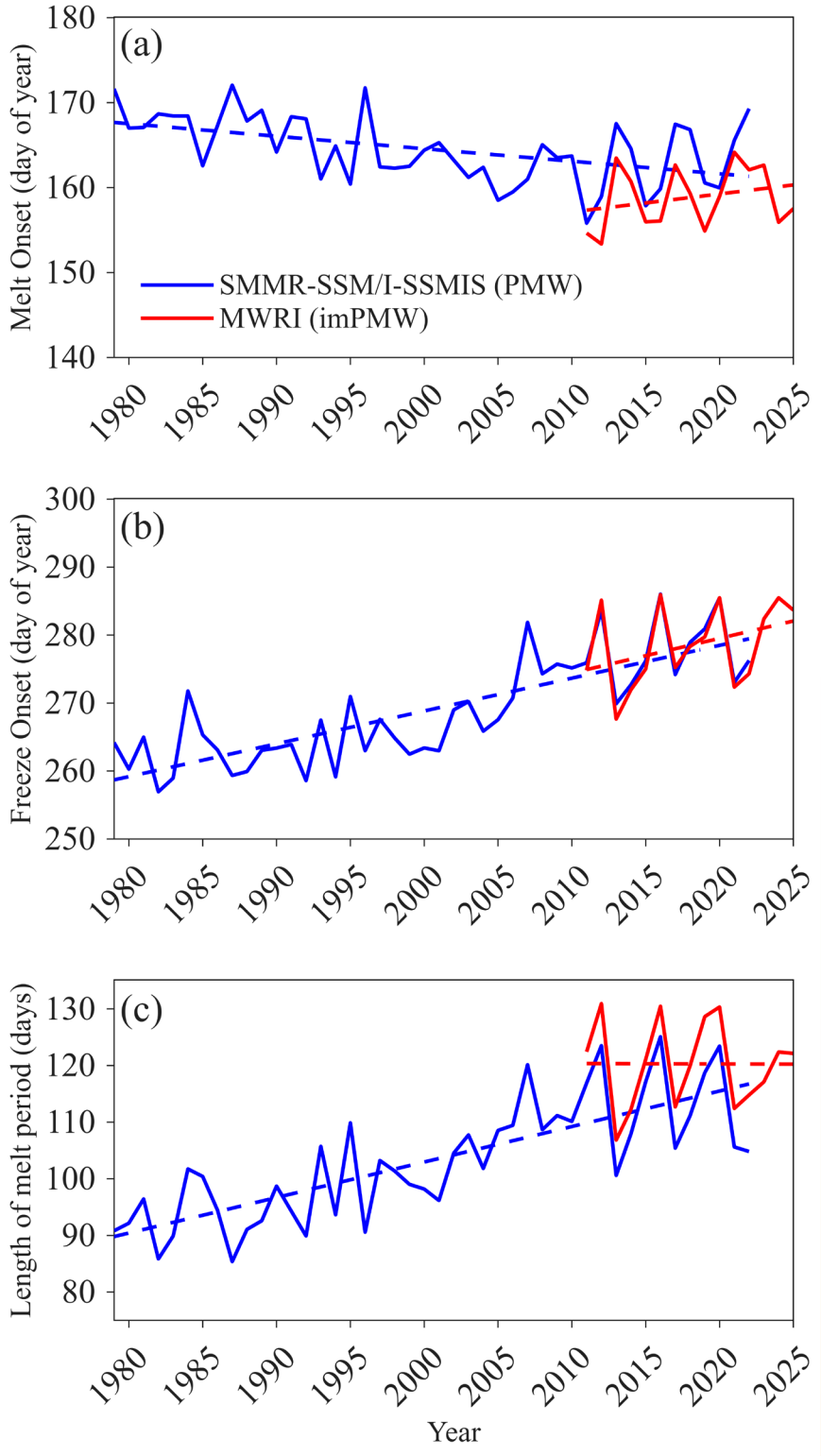

Figure 2.6 Time series of annual averages north of 70°N of (a) the melt onset, (b) the freeze onset, and (c) the melt season length for data from NASA (blue) and OUC (red)

Chapter 3 Atmospheric Composition

3.1 Major Greenhouse Gases

Greenhouse gases refer to natural or anthropogenic gaseous components in the atmosphere that have the ability to absorb and emit longwave radiation from the Earth's surface, atmosphere, and clouds. This characteristic leads to the greenhouse effect. According to the Kyoto Protocol, the major greenhouse gases in the Earth's atmosphere include carbon dioxide (CO_2), methane (CH_4), nitrous oxide (N_2O), as well as sulfur hexafluoride (SF_6), hydrofluorocarbons (HFCs), and perfluorocarbons (PFCs).This section is based on data collected at polar stations from the World Data Centre for Greenhouse Gases (WDCGG) and China's Zhongshan Station. There are 13 stations in Antarctica and 16 stations in the Arctic (Figure 3.1), covering the period from 1984 to 2024 (the concentrations of these greenhouse gases have currently only been published up to 2024). This section mainly analyzes the variations of four major greenhouse gases: carbon dioxide, methane, nitrous oxide, and sulfur hexafluoride.

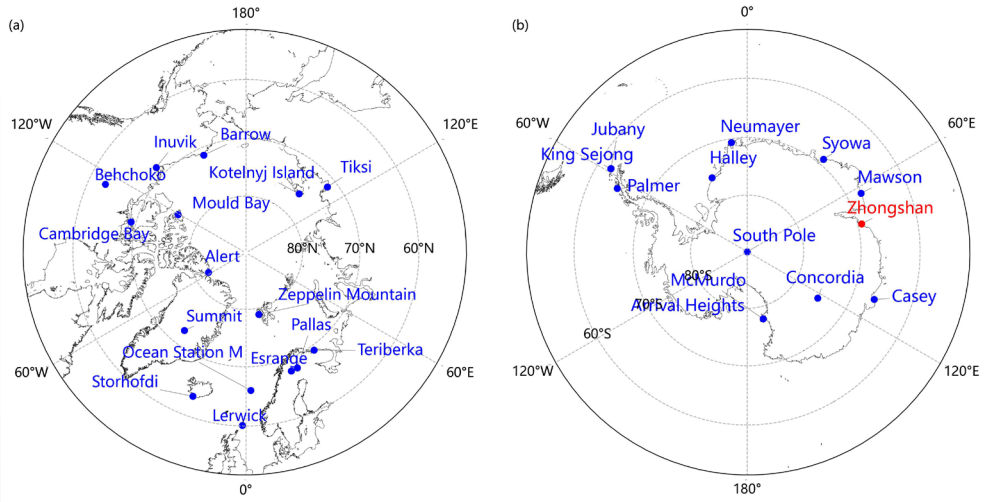

Figure 3.1 Locations of major polar atmospheric composition observation stations

3.1.1 Antarctica

(1) CO_2 and CH_4

From 1984 to 2024, CO_2 concentration in the Antarctic atmosphere showed a steady annual rise, with an average annual absolute increase of 1.92 ppm/year, consistent with the global trend. The average concentration was 3.96 ppm lower than the global mean (Figure 3.2a). In 2024, the annual mean CO_2 concentration in Antarctica reached 419.99 ppm, up 3.6 ppm from 2023. At Zhongshan Station, it was 419.21 ppm.

Similarly, the CH_4 concentration in the Antarctic atmosphere exhibited a steady annual increase, with an average annual absolute increment of 7.27 ppb/year, generally consistent with the global trend. The average

concentration was 65.3 ppb lower than the global average (Figure 3.2b). In 2024, the annual average CH_4 concentration in the Antarctic atmosphere reached 1876.5 ppb, an increase of 5.82 ppb compared to 2023. The annual average CH_4 concentration at Zhongshan Station was 1875.09 ppb.

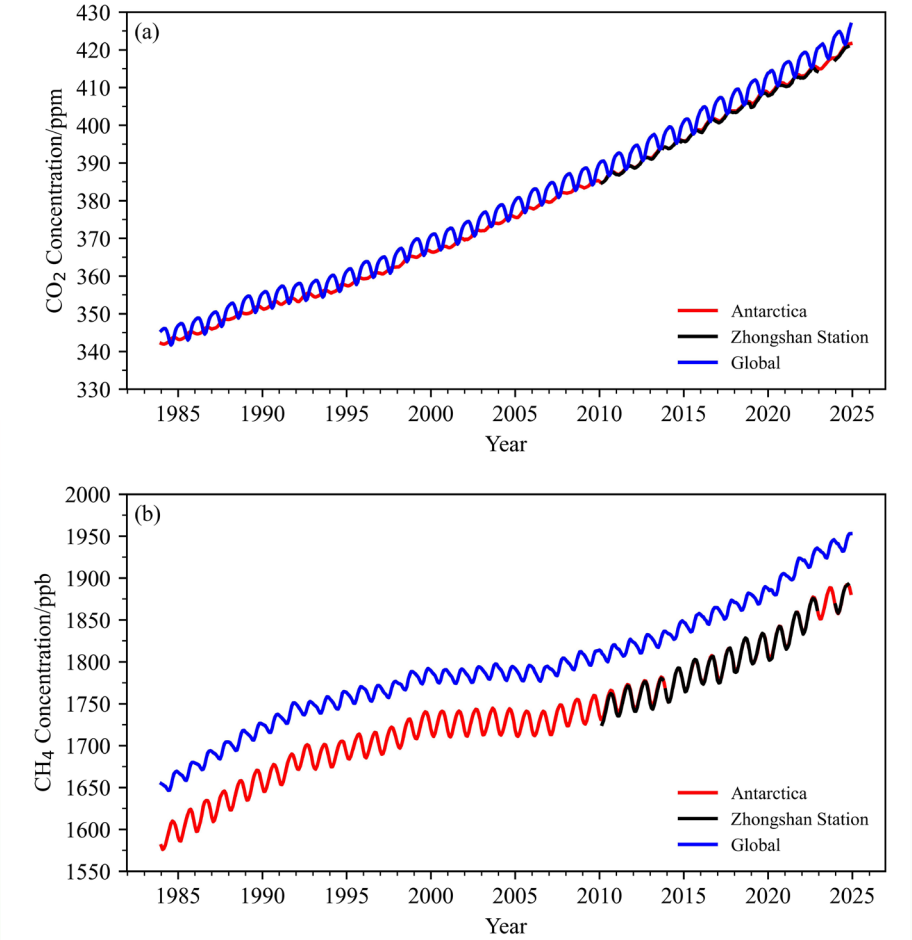

Figure 3.2 Changes in concentrations of CO_2 (a) and CH_4 (b) in Antarctica and the globe, 1984 to 2024

(2) N_2O and SF_6

Currently, data from six Antarctic observation stations monitoring N_2O show that the annual average concentration of N_2O increased from 312.09 ppb in 1997 to 336.80 ppb in 2024, with an average annual absolute increase of 0.91 ppb/year (Figure 3.3a). In 2024, the absolute increase in the annual average concentration of N_2O in Antarctica compared to 2023 was 1.10 ppb, a relative increase of 0.33%, which is lower than the absolute increase of 1.20 ppb from 2022 to 2023, and slightly higher than the average growth rate of the past decade (1.06 ppb/year). Compared to the global level, the absolute increase in the annual average concentration of N_2O in Antarctica from 2023 to 2024 is higher than the global average absolute increase (1.0 ppb).

From 1997 to 2024, only three stations in Antarctica conducted atmospheric SF_6 concentration observations, and the annual average concentrations all showed significant upward trends (Figure 3.3b). The annual average concentration increased from 3.83 ppt in 1997 to 11.55 ppt in 2024, an increase of about threefold, with an average annual absolute increase of 0.29 ppt/year. In 2024, the annual average concentration of SF_6 at the three Antarctic stations increased by 0.40 ppt compared to the 2023 average

concentration, marking the highest year-to-year growth in history.

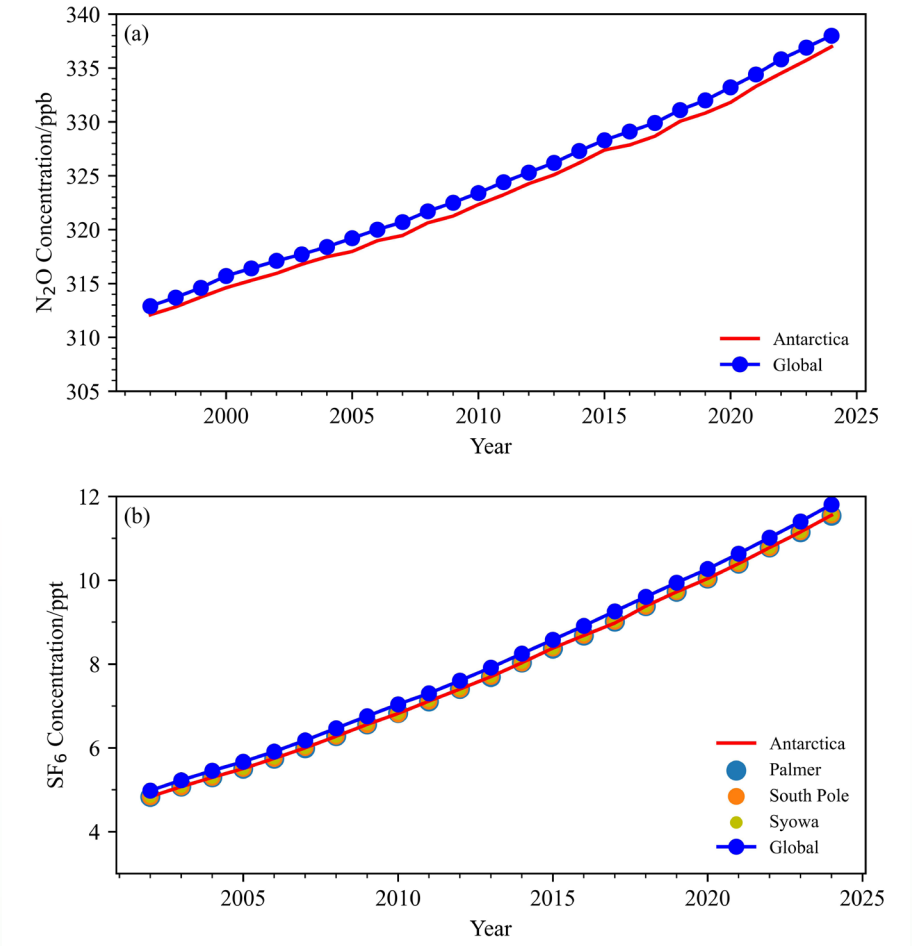

Figure 3.3 Annual average concentrations of (a) N_2O and (b) SF_6 (1997 – 2024) in Antarctica
Note: the global average concentration of SF_6 is from NOAA

3.1.2 Arctic

(1) CO_2 and CH_4

From 1984 to 2024, CO_2 concentration in the Arctic atmosphere showed a steady annual rise, with an average annual absolute increase of 2.01 ppm/year, consistent with the global trend. The average concentration was 2.18 ppm higher than the global mean (Figure 3.3a). In 2024, the annual mean CO_2 concentration in the Arctic reached 426.13 ppm, up 2.94 ppm from 2023.

Similarly, from 1984 to 2024, CH_4 concentration in the Arctic atmosphere showed a steady annual rise, with an average annual absolute increase of 7.6 ppb/year, consistent with the global trend. The average concentration was 82.52 ppb higher than the global mean (Figure 3.3b). In 2024, the annual mean CH_4 concentration in the Arctic reached 2024.33 ppb, up 8.56 ppb from 2023.

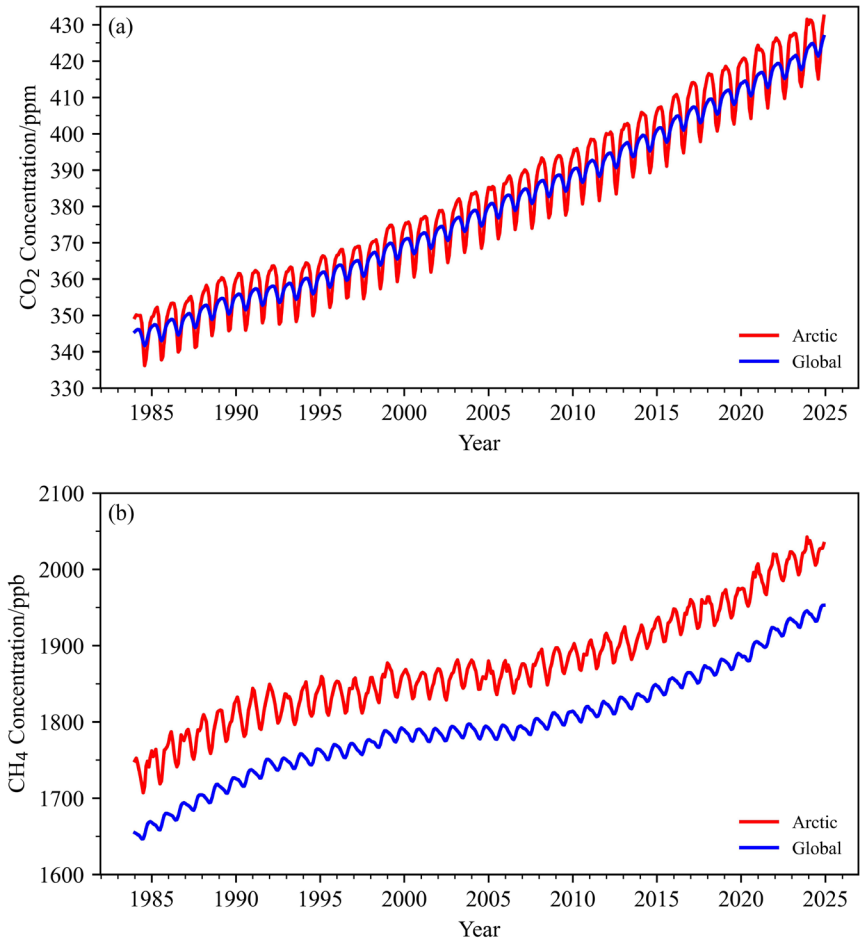

Figure 3.4 Changes in concentrations of CO_2 (a) and CH_4 (b) in in the Arctic and the globe, 1984 to 2024

(2) N_2O and SF_6

Currently, there are six atmospheric baseline stations in the Arctic conducting N_2O observations. The average N_2O concentration at these six stations has increased from 313.31 ppb in 1997 to 338.06 ppb in 2024, with an average annual absolute increase of about 0.90 ppb per year (Figure 3.5a). In 2024, the annual average N_2O concentration in the Arctic rose by 1.02 ppb compared to 2023.

Based on data from six stations conducting SF_6 observations in the Arctic region, the annual average concentration of SF_6 increased from 5.14 ppt in 2002 to 12.05 ppt in 2024, with an average annual absolute increase of 0.31 ppt/year (Figure 3.5b). In 2024, the annual average concentration of SF_6 in the Arctic increased by 0.41 ppt compared to 2023.

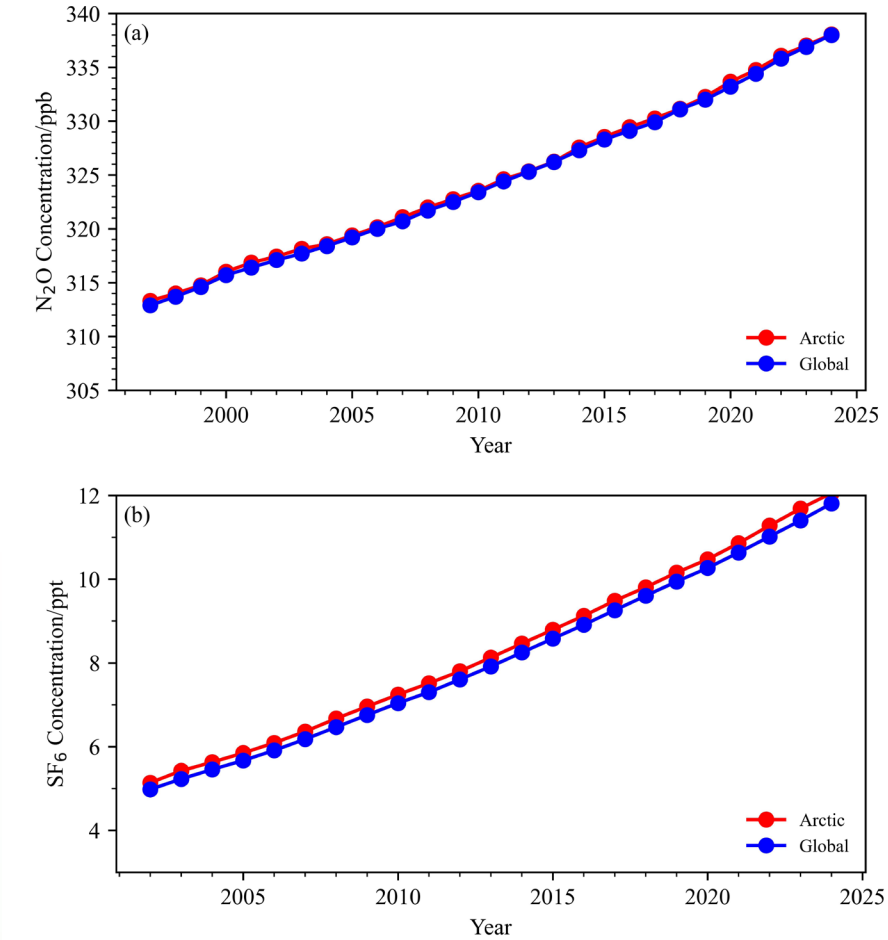

Figure 3.5 Annual average concentrations of (a) N_2O (1997–2024) and (b) SF_6 (2002– 2024) in the Arctic
Note: the global average concentration of SF_6 is from NOAA

3.2 Trace Gases

Trace gases refer to the atmospheric constituents that exist in extremely low concentrations, typically less than 1 ppm. Despite their minuscule proportion in the atmosphere, these gases play a crucial role in climate change, air pollution, and atmospheric chemical processes. Common trace gases include ozone (O_3), carbon monoxide (CO), and nitrogen oxides (NOx). This section analyzes surface ozone monitoring data from polar sites and China's Zhongshan Station, provided by the World Data Center for Reactive Gases (WDCRG). The data includes six stations in Antarctica and four in the Arctic, spanning the period from 1996 to 2024 (the surface ozone concentration data is available up to 2024). The main focus of this section is the temporal and spatial variations of surface ozone concentrations.

3.2.1 Antarctica

In 2024, concentrations at high-latitude inland stations (South Pole Station, Concordia Station) were relatively high, with an average concentration of 30.34 ppb, while those at coastal stations (Zhongshan Station, Halley Station, Neumayer Station, Syowa Station) were relatively low, averaging 22.00 ppb. Among

them, surface ozone concentrations at Zhongshan Station have exhibited a significant downward trend since 2018, with an annual average decline of approximately 0.96 ppb per year, and the average concentration reached 21.15 ppb in 2024. Overall, surface ozone concentrations in the Antarctic show no long-term linear trend, and interannual fluctuations act as the dominant factor (Figure 3.6).

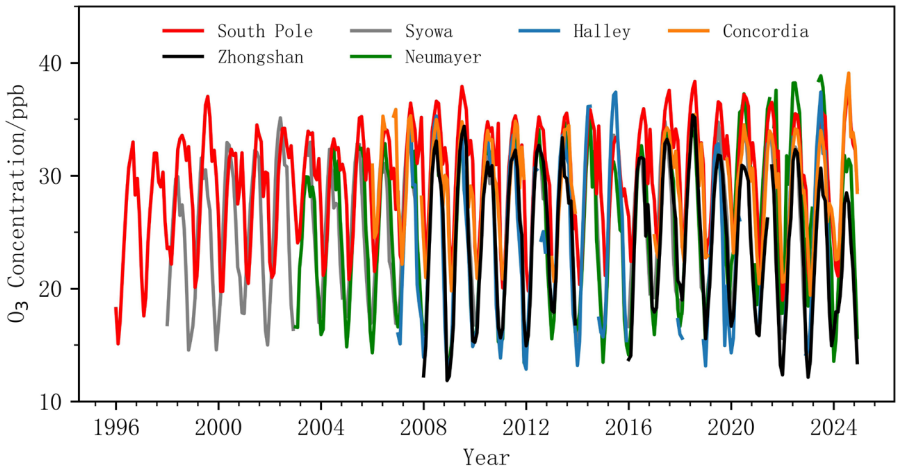

Figure 3.6 Time series of monthly average surface ozone concentrations from 1996 to 2024 at six atmospheric baseline stations in Antarctica

3.2.2 Arctic

In the Arctic, the average concentration of surface ozone observed at four monitoring stations in the Arctic increased from 30.89 ppb in 1999 to 35.26 ppb in 2024, with a changing rate of approximately 0.17 ppb per year. The average surface ozone concentration in the Arctic in 2024 decreased by 0.08 ppb compared with that in 2023, showing no significant long-term linear trend. However, large spatial differences existed in the average surface ozone concentration across different Arctic regions. In 2024, the average surface ozone concentration at Summit Station reached the highest value of 50.70 ppb, while that at Barrow Station was the lowest at 16.19 ppb (Figure 3.7).

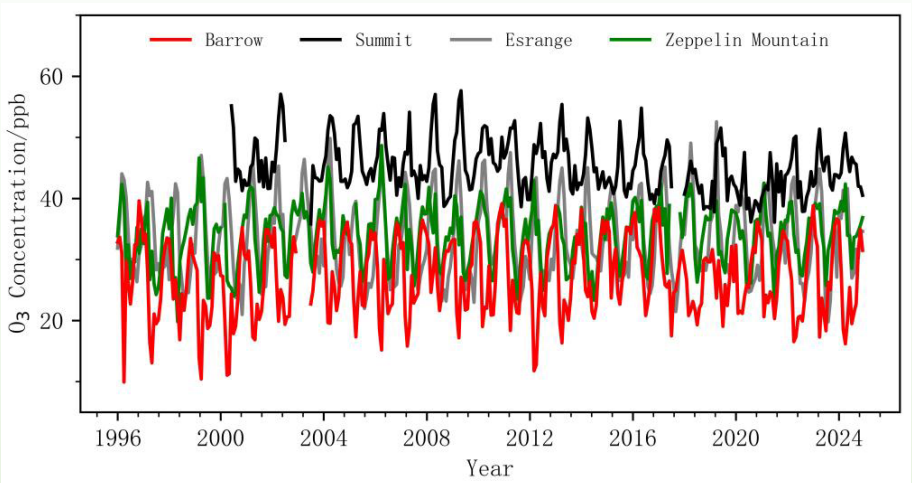

Figure 3.7 Time series of monthly average surface ozone concentrations from 1996 to 2024 at four atmospheric baseline stations in the Arctic

3.3 Total Ozone

3.3.1 Antarctic Ozone Hole

In 2025, the Antarctic ozone hole was generally characterized by a relatively small size, short duration, and early dissipation. In terms of area variation, its maximum single-day coverage reached approximately 22.86 million square kilometers, significantly smaller than the peak level of about 25 million square kilometers recorded in 2022 and 2023, and about 30% smaller than the historical maximum observed in 2006. This made it the fifth smallest Antarctic ozone hole on record since long-term observations began. During the peak period from September 7 to October 13, the average area of the ozone hole was 18.70 million square kilometers, smaller than the long-term average.

From the perspective of its life cycle, the ozone hole began to form in late August, broadly consistent with the long-term average for 1979–2021. It reached its annual maximum around September 9 and closed completely before the end of November, about three weeks earlier than the average closing time of the past decade.

The characteristics of the ozone hole this year were the combined result of the long-term effects of ozone protection efforts and short-term atmospheric variations. On the one hand, a relatively weak polar stratospheric vortex and slightly higher stratospheric temperatures suppressed the formation of polar stratospheric clouds and slowed the chemical reactions that destroy ozone layers, thereby reducing both the size and lifetime of the hole. On the other hand, the long-term implementation of the Montreal Protocol and its amendments have reduced emissions of ozone-depleting substances, continuing to support the gradual recovery of the global ozone layer.

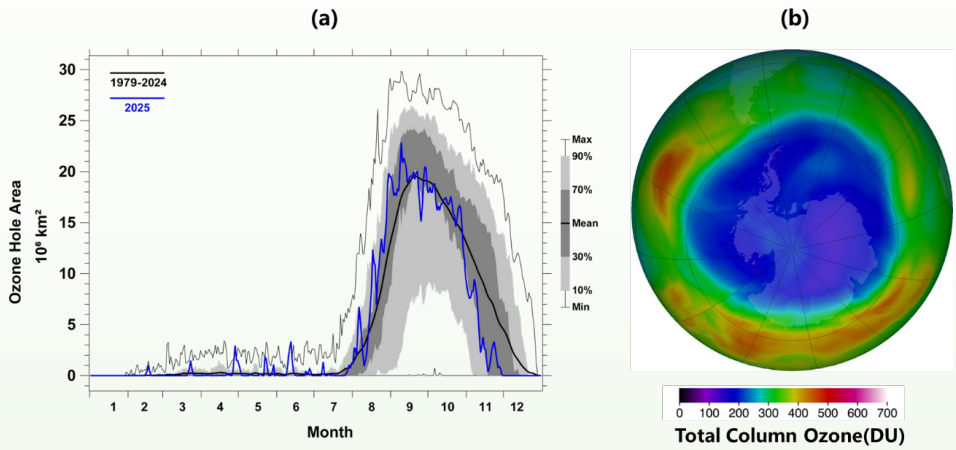

Figure 3.8 (a) Changes in the Southern Hemisphere ozone hole area in 2025 compared with the historical average since 1979; (b) Spatial distribution of the maximum daily extent of the Antarctic ozone hole in 2025

3.3.2 Arctic Ozone Depletion

In spring 2025, the average total ozone over the Arctic was 414 DU, lower than in 2024 and slightly below the average level since 1980. From the winter of 2024 to early spring 2025, the Arctic stratosphere experienced an unusually strong and persistent polar vortex, resulting in a substantial decline in total ozone

in some regions.

In early February 2025, temperatures at the 50 hPa level in the Arctic stratosphere dropped to −94°C, setting an observational extreme in recent years. For most of the month, temperatures remained below the critical threshold for the formation of polar stratospheric clouds (−78°C), leading to extensive activation of ozone-depleting substances such as chlorine and bromine.

In March 2025, total ozone over the Arctic polar region was significantly below the climatological average, and a pronounced low-ozone area appeared over the Scandinavian Peninsula and northern Eurasia. In contrast to the "historically highest" ozone-rich conditions observed during the same period in 2024, Arctic ozone in 2025 showed a typical depletion-type pattern. Although the scale of depletion did not exceed the historical extremes of 2011 and 2020, it was still among the more severe Arctic ozone depletion years in recent decades.

From the perspective of long-term evolution, conditions in 2025 once again confirm the extremely high interannual variability of Arctic stratospheric ozone. Unlike Antarctica, where the ozone layer shows a relatively stable and gradual recovery trend, the Arctic ozone layer is strongly modulated by atmospheric dynamics. In the future, as increasing greenhouse gases continue to cool the stratosphere, Arctic "cold winter" conditions similar to those of 2025, along with associated low-ozone events, may still occur intermittently. Full recovery of Arctic ozone will therefore require several more decades of monitoring and patience.

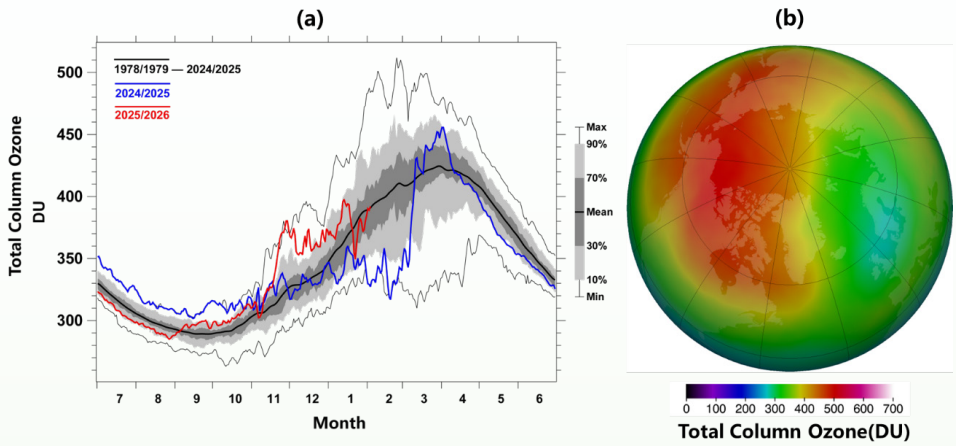

Figure 3.9 (a) Comparison of the average total ozone over the Arctic region in 2025 with the historical average since 1979; (b) Spatial distribution of Arctic ozone column concentration in March 2025

Main Data Sources

1. National Arctic and Antarctic data center (NADC) Meteorological observation products
   https://datacenter.chinare.org.cn/data-center/dindex
2. China Meteorological Administration Global Atmospheric/Land Surface Reanalysis data (CMA-RA)
   http://idata.cma/idata/web/fact/toTechReport2
3. Global Historical Climatology Network - Daily (GHCN-Daily)
   https://www.ncdc.noaa.gov/cdo-web/datasets
4. Global Surface Summary of the Day
   https://registry.opendata.aws/noaa-gsod
5. The British Antarctic Survey
   https://www.bas.ac.uk/project/reader/#data
6. Danish Meteorological Institute
   http://research.dmi.dk/data/
7. The Operational Sea Surface Temperature and Sea Ice Analysis (OSTIA) dataset
   https://data.marine.copernicus.eu/product/SST_GLO_SST_L4_REP_OBSERVATIONS_010_011/description
8. National Snow and Ice Data Center
   https://nsidc.org/data/nsidc-0051/versions/2
9. National Satellite Meteorological Center-FENGYUN Satellite Data
   http://data.nsmc.org.cn/portalsite/default.aspx
10. Daily Sea Ice Concentration of FY-3 MWRI of the -FENGYUN series satellites, provided by Sun Yat-sen University
    http://www.orsc.hellosea.org.cn/#/product-detail?ProductId=1896894818039107586
11. The Earth Science Data Systems of NASA (National Aeronautics and Space Administration)
    https://www.earthdata.nasa.gov/
12. Ocean University of China (OUC)
    http://coas.ouc.edu.cn/pogoc/sjgx/list.htm 11
13. The World Data Centre for Greenhouse Gases (WDCGG)
    https://gaw.kishou.go.jp/publications/global_mean_mole_fractions#content1
14. National Oceanic and Atmospheric Administration（NOAA）
    https://gml.noaa.gov/ccgg/data/getdata.php?gas=SF6
15. The World Data Center for Reactive Gases (WDCRG)
    https://ebas-data.nilu.no
16. Goddard Space Flight Center of NASA (National Aeronautics and Space Administration)
    https://ozonewatch.gsfc.nasa.gov/

Glossary

Antarctica: The vast region south of latitude 60°S.

Arctic: The vast region north of latitude 60°N.

Anomaly: The difference between a variable and its multi-year average value for the period 1991 to 2020.

Reanalysis Data: Historical weather data obtained by assimilating model forecasts and observational data through advanced, fixed assimilation systems and numerical forecast models to produce a rich dataset with complete spatial coverage and consistent time series. In this report, reanalysis data specifically refers to the first-generation global atmospheric reanalysis dataset, CMA-RA, released by the National Meteorological Information Center.

Southern Ocean: Refers to a unique body of water that surrounds the Antarctic continent and has no land boundary to the north. It is composed of parts of the South Pacific, South Atlantic and South Indian Oceans, together with the Weddell Sea, Ross Sea, Amundsen Sea and Bellingshausen Sea around the Antarctic continent, covering the area south of 50°S.

The Arctic Ocean: Its main body is located north of the Arctic Circle (66.5°N), and the latitude of its core sea area ranges from 65°N to 90°N.

Antarctic Oscillation(AAO): The seesaw change phenomenon of the pressure field between the Antarctic and the mid-latitudes of the Southern Hemisphere, also known as the Southern Hemisphere Annular Model (SAM), is one of the main characteristic modes of atmospheric circulation in the Southern Hemisphere.

Arctic Oscillation(AO): The seesaw change phenomenon of the air pressure field between the Arctic and the mid-latitudes of the Northern Hemisphere, also known as the Northern Hemisphere Annular Mode(NAM), is one of the main characteristic modes of atmospheric circulation in the Northern Hemisphere.

AAO/AO index: Using CMA-RA reanalysis data, it is calculated based on the difference in zonal mean sea level pressure between the polar area and the middle latitudes (Li et al,2003). The AO index is the difference between 35°N and 65°N, and the AAO index is the difference between 40°S and 70°S.

Polar Vortex: a large-scale low-pressure vortex phenomenon in the polar troposphere and stratosphere, which has an important impact on the climate of the polar regions and mid-high latitudes of the northern and southern hemispheres.

Arctic Polar Vortex Index: Indicators used to describe and measure the characteristics and changes of the Arctic polar vortex.

Sea ice concentration: a measurement of the amount of sea ice in a given area, usually described as a percentage.

Sea ice extent: the total region with at least 15 percent sea ice concentration.

Melt Onset(MO): Free water is continuously present with in the snow pack and the ice surface becomes

damp at the snow ice interface.

Freeze Onset(FO): The ice is generally bare to lightly snow covered, well drained and the surface layer of the ice is refrozen.

Greenhouse gases: Natural or anthropogenic gas components in the atmosphere that can absorb and emit longwave radiation from the Earth's surface, atmosphere, and clouds, leading to the greenhouse effect. The major greenhouse gases in the Earth's atmosphere include carbon dioxide (CO_2), methane (CH_4), nitrous oxide (N_2O), sulfur hexafluoride (SF_6), hydrofluorocarbons (HFCs), and perfluorocarbons (PFCs), as specified in the Kyoto Protocol.

PPM: The number of molecules of a given gas per million (10^6) molecules of dry air.

PPB: The number of molecules of a given gas per billion (10^9) molecules of dry air.

PPT: The number of molecules of a given gas per trillion (10^{12}) molecules of dry air.

Greenhouse Gases observation stations in Arctic: Kotelny Island Station (Russia, KOT), Tiksi Station (Russia, TIK), Alert Station (Canada, ALT), Mould Bay Station (Canada, MBC), Barrow Station (USA, BRW), Behchokǫ̀ Station (Canada, BCK), Cambridge Bay Station (Canada, CBY), Inuvik Station (Canada, INU), Zeppelin Mountain Station (Norway, ZEP), Summit Station (Denmark, SUM), Teriberka Station (Russia, TER), Pallas Station (Finland, PAL), Storhofdi Station (Iceland, ICE), Lerwick Station (UK, SIS), Ocean Station M (Norway, STM).

Greenhouse Gases observation stations in Antarctica: King Sejong Station (South Korea, KSG), Jubany Station (Argentina, JBN), Palmer Station (USA, PSA), Casey Station (Australia, CYA), Mawson Station (Australia, MAA), Showa Station (Japan, SYO), Halley Station (UK, HBA), Arrival Heights Station (New Zealand, ARH), McMurdo Station (USA, MCM), South Pole Station (USA, SPO), Zhongshan Station (China, ZOS).

Dobson unit (DU): A unit to measure the total amount of ozone in a vertical column above the Earth's surface (total column ozone). The number of Dobson Units is the thickness in units of 10^{-5} m that the ozone column would occupy if compressed into a layer of uniform density at a pressure of 1013 hPa and a temperature of 0°C. One DU corresponds to a column of ozone containing 2.69×10^{20} molecules per square metre. A typical value for the amount of ozone in a column of the Earth's atmosphere, although very variable, is 300 DU.

Ozone-depleting substances (ODSs): Ozone-depleting substances (ODSs) are man-made gases that destroy ozone (O_3) once they reach the ozone layer in the stratosphere. Ozone depleting substances include: chlorofluorocarbons (CFCs), hydrochlorofluorocarbons (HCFCs), hydrobromofluorocarbons (HBFCs), halons, methyl bromide, carbon tetrachloride and methyl chloroform.

Ozone layer: The ozone layer is a layer of Earth's stratosphere that absorbs most of the Sun's ultraviolet radiation. It contains high concentrations of ozone (O_3) in relation to other parts of the atmosphere, although still small in relation to other gases in the stratosphere.The ozone layer is mainly found in the lower portion of the stratosphere, from approximately 12 to 40 kilometres above Earth, and reach the maxima from 20 to 25 kilometres. Every year, during the spring of the Southern Hemisphere, the ozone layer over the Antarctic region experiences very strong depletion, caused by anthropogenic chlorides and bromides in combination with the region's specific meteorological conditions. This phenomenon is known as the ozone hole.

STATE OF POLAR CLIMATE
2025